Stability and Bautin bifurcation of four-wheel-steering vehicle system with driver steering control

Pengcheng Miao[a], Denghui Li[b], Yuan Yue[c] *, Celso Grebogi[d]

[a] School of Mechanical Engineering, Yangtze University, Jingzhou 434023, China

[b] School of Mathematics and Statistics, Hexi University, Zhangye 734000, China

[c] School of Mechanics and Aerospace Engineering, Southwest Jiaotong University, Chengdu 610031, China

[d] Institute for Complex Systems and Mathematical Biology King's College, University of Aberdeen, Aberdeen AB24 3UE, United Kingdom

Abstract

In this paper, the stability and Bautin bifurcation of a four-wheel-steering(4WS) vehicle system, by considering driver steering control, are investigated. By using the central manifold theory and projection method, the first and second Lyapunov coefficients are calculated to predict the type of Hopf bifurcation of the vehicle system. The topological structure of the Bautin bifurcation, a degenerate Hopf bifurcations of the 4WS vehicle system is presented in the parameter space and it reveals the dynamics of the vehicle system of different choices of the control parameters. The influences of system parameters on critical values of the bifurcation parameter are also analyzed. It is shown that with the increase of the frontal visibility distance of the driver control strategy coefficient and the cornering stiffness coefficients of the rear wheels, the critical speed increases. Nevertheless, the critical speed decreases with the increase of the distance from the center of gravity of the vehicle to the front axles, Driver's perceptual time delay, and cornering stiffness coefficients of the front wheels.

Keywords: 4WS vehicle; stability analysis; Bautin bifurcation; center manifold; projection method.

Lead Paragraph

The four-wheel-steering (4WS) technique can improve the flexibility, stability and safety of the vehicle's steering. Thus, it has been developed rapidly in the past decades. In this work, we analyze the stability and bifurcation of a 4WS vehicle/driver closed-loop system. The topological structure of the Bautin bifurcation of the 4WS vehicle system is presented in the parameter space. The study of the lateral dynamics for the system allowed a prediction of the 4WS vehicle behavior after the loss of linear stability and reveal the transition mechanism between supercritical and subcritical Hopf bifurcation of the 4WS vehicle system.

*Corresponding author, E-mail: leyuan2003@sina.com

1 Introduction

As an important means of transportation, the automobile plays an crucial role in a country's economy and in our way of life. With the development of modern highway network and advancement of vehicle running speed, the investigation of vehicle system lateral dynamics has attracted more and more attention by researchers [1, 2]. The nonlinear dynamics, being at core in the study of stability of vehicle systems, is a very significant topic. In the research of lateral dynamics of vehicle system, the nonlinearity mainly comes from geometric nonlinearity and tyre force nonlinearity. The research on lateral stability, bifurcation and chaotic dynamics of two-wheel-steering (2WS) vehicle system has been extensive and in-depth [3, 4]. However, when the high-speed vehicle with only two front wheels steering turns, the rear of the vehicle body often produces a large tail swing and sideslip, which seriously affects the safety of the vehicle. Compared with the traditional front-wheel-steering vehicle, the 4WS vehicle has the advantages of excellent stability at high speed and high sensitivity at low speed. In order to meet the driver's requirements for flexibility, comfort and safety of the automobile, the 4WS system has been studied since the 1980s [5, 6, 7]. Dai and Han [8] established a two-degrees of freedom 4WS vehicle/driver closed-loop system, studied the stability and Hopf bifurcation of the system by using bifurcation analysis, and discussed the influence of driver parameters on vehicle stability. Hu [9] presented a 4WS vehicle system with delay in driver's response and analyzed the asymptotic stability and Hopf bifurcation of the system. It was shown that the 4WS vehicle has better performance stability than the 2WS vehicle, and the bilinear control strategy works better than the linear control strategy when considering time delay in the driver's response. Shen et al. [10] investigated the nonlinear dynamics of the 4WS vehicle system without considering the driver's response by using joint-point locus geometric approach. It was found that the difference between the front and the rear steering angles plays a key role in 4WS vehicle system dynamics and the system exhibits complex dynamical behavior for extremely large steering angles. Nguyen et al. [11] studied the lateral load transfer effects on dynamics of 4WS vehicle system. It was shown that the adjusting of the roll moment distribution can alter the bifurcation locations for oversteering vehicles. Rossa at al. [12] presented a simple mathematical model describing a vehicle with driver's response, and performed a three-parameter bifurcation analysis.

Numerous research works on the stability and Hopf bifurcation of 4WS vehicle system have been carried out since the first 4WS vehicle system was reported [8, 9]. However, the degenerate Hopf bifurcation, named Bautin bifurcation, which is a codimension-two bifurcation, has lacked attention for the 4WS vehicle system. In this work, we focus on the stability and Bautin bifurcation analysis for a 4WS vehicle/driver closed-loop system with the nonlinearity from lateral tyre force and geometric nonlinearity.

The remainder of this paper is organized as follows. In Section 2, the dynamical model of the vehicle/driver system is described and the steady state motion of the system is analyzed. In Section 3, the stability and Bautin bifurcation of the 4WS vehicle system are analyzed. In Section 4, numerical calculation and simulations are carried out to validate the theoretical analysis, and the effects on parameter changes in the dynamics of the vehicle system are investigated. In

Section 5, the main conclusions drawn in this work are provided.

2 Dynamics of vehicle/driver model

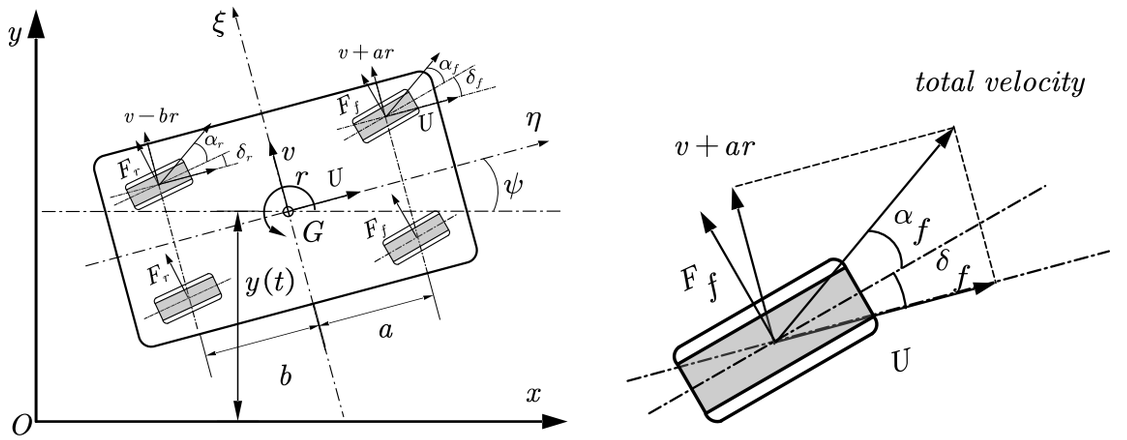

(a) The vehicle in a frame of coordinate

(b) Zoom view of a front wheel

Fig. 1 Model of 4WS vehicle system and the coordinate system.

We consider the nonlinear dynamics of vehicle/driver model shown in Fig. 1. It is assumed that the 4WS vehicle system is a rigid body with mass m, and the mass is symmetrically distributed on the four wheels. The forward speed along the tangent direction of the vehicle trace is denoted as U. In this work, the effects of roll motion and vertical motion are ignored and only lateral dynamics are considered. Therefore, the system has two degrees of freedom, lateral motion and yaw motion. Two coordinate system is established as shown in Fig. 1(a), where (η, ξ) represents the body coordinate system; the origin of the coordinate G is the center of mass of the vehicle and (x, y) represents the fixed coordinate system. The motion equations of the vehicle system are as follows [8]:

$$\begin{aligned} m(\dot{v} + rU) &= 2F_f \cos\delta_f + 2F_r \cos\delta_r, \\ I_z\dot{r} &= 2aF_f \cos\delta_f - 2bF_r \cos\delta_r, \end{aligned} \tag{2.1}$$

where v and r are the lateral and yaw velocities in the local coordinate system, respectively, m is the mass of the vehicle, I_z is the inertia moment of rotation of the vehicle body with respect to the vertical axis z, a and b are the distances from the center of mass to the front and rear axles, respectively, δ_f and δ_r are the steering angles applied on the front and rear wheels, respectively. The terms F_f and F_r represent the lateral forces acting on the front and rear wheels of the vehicle due to the contact between the tyres and the road surface. The lateral force is a function of the physical properties of the tyres and of the sideslip angles (α_f, α_r) proposed by Sachs and Chou [13]. The sideslip angles can be obtained from simple geometric relations shown in Fig.1

(b) as follows:

$$\begin{aligned} \alpha_f &= \arctan(\frac{v+ar}{U}) - \delta_f, \\ \alpha_r &= \arctan(\frac{v-br}{U}) - \delta_r. \end{aligned} \tag{2.2}$$

A large number of works have been made on tyre force modelling [14] which affects the lateral dynamics of vehicle system. One of the better known is the Magic Formula proposed in [15]. In order to facilitate the application of nonlinear dynamics theory to analyze the dynamics of vehicle system, the cubic polynomials tyre force model is used in this paper. Its mathematical model is described as follows:

$$\begin{aligned} F_f &= -C_1\alpha_f + C_3\alpha_f^3, \\ F_r &= -D_1\alpha_r + D_3\alpha_r^3, \end{aligned} \tag{2.3}$$

where C_1, C_2, D_1 and D_2 are the parameters, cornering stiffness coefficients, determined by the experiments as described in [4].

In order to ensure the stability of the car at high speed, much research on the control strategy has been carried out [7, 16]. In this work, the linear control strategy is being used, which is mathematically expressed as

$$\delta_r = K_L\delta_f, \tag{2.4}$$

where K_L is the control strategy proportionality coefficient.

In the fixed frame, the position of the mass center G of the vehicle is denoted by $(x(t), y(t))$ and the heading angle of the vehicle is represented by ψ. Then, we can obtain the following relation,

$$\dot{\psi} = r, \dot{y} = U\sin\psi + v\cos\psi. \tag{2.5}$$

In the 4WS vehicle system, the driver's control behaviour is another important factor that affects the dynamics of the closed-loop vehicle system. The influence of the driver on the motion state of the vehicle is achieved by controlling the steering angle $\delta_f(t)$ that changes the sideslip angles of the wheels, and thus adjusts the lateral force exerted by the ground on the tyre. However, it is not easy to accurately model the driver behavior quantitatively. Because the driver's behavior is not only affected by objective factors, such as the vehicle, weather, road conditions, and so forth, but also by the driver's own factors, such as experience and physiological state. Different models of driver's behavior have been proposed [17, 18, 19]. In the present work, a simplified pilot model proposed by Legouis et al. [20] is used. When the driver perceives a lateral deviation of the vehicle with respect to the center line of the road at a visibility distance L_d, the driver tries to control the vehicle with a steering angle of $\delta_f(t)$ in order to adjust the vehicle to reduce the lateral deviation, by introducing a loop gain K, the frontal visibility of the driver L_d, and a perceptual time delay T_r, the pilot model can be expressed as the following differential equation [4, 20] with no time delay:

$$\dot{\delta}_f(t) = -\frac{1}{T_r}\left[K\left(y + \frac{L_d}{U}\dot{y}\right) + \delta_f(t)\right]. \tag{2.6}$$

Combining the equations (2.1)-(2.6), we obtain the following governing equation of the vehicle/driver system:

$$\dot{\boldsymbol{x}} = \boldsymbol{f}(\boldsymbol{x}, \boldsymbol{\mu}), \quad \boldsymbol{x} \in \mathbb{R}^5, \tag{2.7}$$

where

$$\begin{aligned}
\boldsymbol{x} =&(v, r, y, \psi, \delta_f)^T = (x_1, x_2, x_3, x_4, x_5)^T,\\
\boldsymbol{f} =&(f_1, f_2, f_3, f_4, f_5)^T,\\
f_1 =&\frac{2}{m}[F_f \cos x_5 + F_r \cos K_L x_5] - U x_2,\\
f_2 =&\frac{2}{I_z}[aF_f \cos x_5 - bF_r \cos K_L x_5],\\
f_3 =&x_1 \cos x_4 + U \sin x_4,\\
f_4 =&x_2,\\
f_5 =&-\frac{1}{T_r}\left[Kx_3 + \left(\frac{KL_d}{U}\right) x_1 \cos x_4 + KL_d \sin x_4 + x_5\right].
\end{aligned}$$

$\boldsymbol{\mu} = (a, b, I_z, ...)$ represents the set of all physical parameters. The sideslip angles given by (2.2) are rewritten as follows:

$$\begin{aligned}
\alpha_f =&\arctan(\frac{x_1 + ax_2}{U}) - x_5,\\
\alpha_f =&\arctan(\frac{x_1 - bx_2}{U}) - K_L x_5.
\end{aligned}$$

It is worth noting that the vector field $\boldsymbol{f}(\boldsymbol{x}, \boldsymbol{\mu})$ has symmetric property, that is, $\boldsymbol{f}(-\boldsymbol{x}, \boldsymbol{\mu}) = -\boldsymbol{f}(\boldsymbol{x}, \boldsymbol{\mu})$.

2.1 Steady state motion

Let the right-hand side of the equation (2.7) equal to zero, we obtain a set of nonlinear algebraic equations for governing the equilibrium points of the vehicle system (2.7) as follows:

$$\begin{cases}
F_f \cos x_5 + F_r \cos K_L x_5 = 0,\\
aF_f \cos x_5 - bF_r \cos K_L x_5 = 0,\\
x_1 \cos x_4 + U \sin x_4 = 0,\\
x_2 = 0,\\
x_5 + Kx_3 = 0.
\end{cases} \tag{2.8}$$

The system (2.7) has a trivial equilibrium point, $\boldsymbol{x_e} = \boldsymbol{0}$. According to the geometric constrains of $|\delta_f| < \pi/2, |K_L \delta_f| < \pi/2$, and since $a > 0, b > 0$, the first two equations of (2.8) are reduced to the following:

$$\begin{cases}
F_f(x_1, 0, x_5) = 0,\\
F_r(x_1, 0, x_5) = 0.
\end{cases} \tag{2.9}$$

When $|\psi| < \pi/2$, Eq. (2.8) is further simplified as follows:

$$\begin{cases} C_1(x_4+x_5) - C_3(x_4+x_5)^3 = 0, \\ D_1(x_4+K_Lx_5) - D_3(x_4+K_Lx_5)^3 = 0, \\ x_1 = -U\tan x_4, \\ x_2 = 0, \\ x_5 + Kx_3 = 0. \end{cases} \tag{2.10}$$

If $K_L \neq 1$, we obtain eight non-trivial solutions [8] from Eq. (2.10) as follows:

$$\boldsymbol{X_1} = \left(\pm U\tan(\frac{T}{1-K_L}), 0, \mp\frac{T}{K(1-K_L)}, \mp\frac{T}{1-K_L}, \pm\frac{T}{1-K_L}\right)^T,$$
$$\boldsymbol{X_2} = \left(\pm U\tan(\frac{K_LS}{1-K_L}), 0, \mp\frac{S}{K(1-K_L)}, \mp\frac{K_LS}{1-K_L}, \pm\frac{S}{1-K_L}\right)^T,$$
$$\boldsymbol{X_3} = \left(U\tan\big(\frac{1}{1-K_L}[K_LS \mp T]\big), 0, \frac{1}{K(1-K_L)}[S \pm T], \frac{1}{1-K_L}[-K_LS \pm T], \frac{1}{1-K_L}[S \mp T]\right)^T,$$
$$\boldsymbol{X_4} = \left(U\tan\big(\frac{1}{1-K_L}[-K_LS \mp T]\big), 0, \frac{1}{K(1-K_L)}[-S \pm T], \frac{1}{1-K_L}[K_LS \pm T], \frac{1}{1-K_L}[-S \mp T]\right)^T,$$

where $S = \sqrt{\frac{C_1}{C_3}}, T = \sqrt{\frac{D_1}{D_3}}$.

3 Stability analysis and Bautin bifurcation of the trivial equilibrium point

3.1 Stability and Hopf bifurcation analysis

Expanding Eq.(2.7) into a multidimensional Taylor series in x_i about the trivial equilibrium point $\boldsymbol{x_e}$ up to order five, it yields,

$$\dot{\boldsymbol{x}} = \boldsymbol{A}(\boldsymbol{\mu})\boldsymbol{x} + \boldsymbol{g}(\boldsymbol{x},\boldsymbol{\mu}) + \boldsymbol{h}(\boldsymbol{x},\boldsymbol{\mu}) + \boldsymbol{O}(|\boldsymbol{x}|^7), \tag{3.1}$$

where $\boldsymbol{A_\mu}$ is the Jacobian matrix of the vector field $\boldsymbol{f}(\boldsymbol{x},\boldsymbol{\mu})$ computed at the trivial equilibrium point $\boldsymbol{x_e}$, $\boldsymbol{g}(\boldsymbol{x},\boldsymbol{\mu}) = (g_1,g_2,g_3,g_4,g_5)^T$ represents the nonlinear terms of order three in x_i, and $\boldsymbol{h}(\boldsymbol{x},\boldsymbol{\mu}) = (h_1,h_2,h_3,h_4,h_5)^T$ is the nonlinear terms of order five in x_i. Because the vector field $\boldsymbol{f}(\boldsymbol{x},\boldsymbol{\mu})$ for the system(2.7) has the symmetry $\boldsymbol{f}(-\boldsymbol{x},\boldsymbol{\mu}) = -\boldsymbol{f}(\boldsymbol{x},\boldsymbol{\mu})$, the expansion (3.1) has only odd order terms the x_i. The expressions for the matrix $\boldsymbol{A}(\boldsymbol{\mu})$, and the functions $g_i(i=1,\cdots,5), h_i(i=1,\cdots,5)$ are given as in the Appendix.

The characteristic equation of the matrix $\boldsymbol{A}(\boldsymbol{\mu})$ can be expressed as follows:

$$a_0\lambda^5 + a_1\lambda^4 + a_2\lambda^3 + a_3\lambda^2 + a_4\lambda + a_5 = 0, \tag{3.2}$$

where the items $a_i(i=0,\cdots,5)$ can be seen in the Appendix.

As the physical parameters are changed, the roots of Eq. (3.2) move in the complex plane in a complicated way, which affects the stability of the vehicle system. The trivial equilibrium

point $\boldsymbol{x_e} = 0$ is stable if all the roots of Eq.(3.2) have negative real parts. None of the roots of Eq. (3.2) is zero since $a_5 \neq 0$ and $K_L \neq 0$. Therefore, the trivial equilibrium point loses stability only if Eq.(3.2) has a pair of imaginary roots $\lambda = \pm i\omega$. The Hurwitz mtrix of the characteristic Eq. (3.2) is

$$\boldsymbol{H} = \begin{bmatrix} -\frac{2(C_1+D_1)}{mU} & -U - \frac{2(aC_1-bD_1)}{mU} & 0 & 0 & \frac{2}{m}(C_1 + K_L D_1) \\ -\frac{2(aC_1-bD_1)}{I_z U} & -\frac{2(a^2C_1+b^2D_1)}{I_z U} & 0 & 0 & \frac{2}{I_z}(aC_1 - bK_L D_1) \\ 1 & 0 & 0 & U & 0 \\ 0 & 1 & 0 & 0 & 0 \\ -\frac{KL_d}{T_r U} & 0 & -\frac{K}{T_r} & -\frac{KL_d}{T_r} & -\frac{1}{T_r} \end{bmatrix}.$$

The forward speed U of the vehicle is taken as the control parameter, which plays a key role in the stability of the 4WS vehicle system. According to the criterion for the Hopf bifurcation proposed in [21], the sufficient conditions for the Hopf bifurcation are as follows:

$$\begin{aligned} &(\mathrm{H}_1) \quad a_5 > 0, \Delta_1(U_c) > 0, \Delta_2(U_c) > 0, \Delta_3(U_c) > 0, \Delta_4(U_c) = 0, \\ &(\mathrm{H}_2) \quad \left.\frac{d\Delta_4(U)}{dU}\right|_{U=U_c} \neq 0, \end{aligned}$$

where $\Delta_1(U) = a_1, \Delta_2(U) = a_1a_2 - a_3, \Delta_3(U) = a_1(a_2a_3 - a_1a_4) - a_3^2 + a_1a_5$, and $\Delta_4(U) = a_1(a_2a_3a_4 - a_2^2a_5 - a_1a_4^2 + a_4a_5) - a_3^2a_4 + a_2a_3a_5 + a_1a_4a_5 - a_5^2$.

Note that the critical speed U_c can be obtained from the equation $\Delta_4(U_c) = 0$. The condition H_1 implies that the Jacobian matrix $\boldsymbol{A}(U_c)$ of the system has a simple pair of purely complex imaginary eigenvalues, and other eigenvalues have negative real parts. The condition H_2 is equivalent to the transversality condition. We rewrite Eq. (3.1) in the following general form,

$$\dot{\boldsymbol{x}} = \boldsymbol{A}(\boldsymbol{\mu})\boldsymbol{x} + \boldsymbol{F}(\boldsymbol{x}), \qquad \boldsymbol{x} \in \mathbb{R}^5, \tag{3.3}$$

where $\boldsymbol{F}(\boldsymbol{x}) = O(\| \boldsymbol{x} \|^2)$ is a smooth vector function representing the nonlinear terms. Write its Taylor expansion near the trivial equilibrium point $\boldsymbol{x_e} = 0$ as

$$\boldsymbol{F}(\boldsymbol{x}) = \frac{1}{3!}\boldsymbol{C}(\boldsymbol{x},\boldsymbol{x},\boldsymbol{x}) + \frac{1}{5!}\boldsymbol{E}(\boldsymbol{x},\boldsymbol{x},\boldsymbol{x},\boldsymbol{x},\boldsymbol{x}) + O(\| \boldsymbol{x} \|^7), \tag{3.4}$$

where $\boldsymbol{C}(\boldsymbol{x},\boldsymbol{x},\boldsymbol{x})$ and $\boldsymbol{E}(\boldsymbol{x},\boldsymbol{x},\boldsymbol{x},\boldsymbol{x},\boldsymbol{x})$ are symmetric multilinear vector functions. They have the following form in the coordinates $(\gamma, \delta, ...)$,

$$\begin{aligned} C_i(\boldsymbol{\xi},\boldsymbol{\eta},\boldsymbol{\zeta}) &= \sum_{j,k,l=1}^{5} \left.\frac{\partial^3 F_i(x)}{\partial x_j x_k x_l}\right|_{x=0} \xi_j\eta_k\zeta_l, (i = 1,2,3,4,5), \\ E_i(\boldsymbol{\gamma},\boldsymbol{\delta},\boldsymbol{\xi},\boldsymbol{\eta},\boldsymbol{\zeta}) &= \sum_{j,k,l,m,s=1}^{5} \left.\frac{\partial^5 F_i(x)}{\partial x_j x_k x_l x_m x_s}\right|_{x=0} \gamma_j\delta_k\xi_l\eta_m\zeta_s, (i = 1,2,3,4,5). \end{aligned}$$

According to [22], the type of Hopf bifurcation that occurs in the 4WS vehicle system can be deduced by calculating the first Lyapunov coefficient $l_1(0)$ at the critical speed U_c. Introduce a complex eigenvector $\boldsymbol{q} \in \mathbb{C}^5$ of $\boldsymbol{A}(U_c)$ corresponding to the eigenvalue $\lambda_1 = i\omega_0, \omega_0 > 0$ and a

complex eigenvector $\boldsymbol{p} \in \mathbb{C}^5$ of $\boldsymbol{A}^T(U_c)$ corresponding to the eigenvalue $\lambda_2 = -i\omega_0$. Then the two complex eigenvectors satisfy

$$\boldsymbol{A}(U_c)\boldsymbol{q} = i\omega_0\boldsymbol{q}, \boldsymbol{A}^T\boldsymbol{p} = -i\omega_0\boldsymbol{p}. \tag{3.5}$$

Then normalize $\boldsymbol{p}$ with respect to $\boldsymbol{q}$: $\langle \boldsymbol{p}, \boldsymbol{q} \rangle = 1$, where$\langle \boldsymbol{p}, \boldsymbol{q} \rangle = \sum_{i=1}^{5} \bar{p}_i q_i$.

Following [22] and imposing the symmetry of the vehicle system (3.3), the first Lyapunov coefficient $l_1(0)$ can be calculated by the formula

$$l_1(0) = \frac{1}{2\omega_0} Re(\langle \boldsymbol{p}, \boldsymbol{C}(\boldsymbol{q}, \boldsymbol{q}, \bar{\boldsymbol{q}}) \rangle) \tag{3.6}$$

If $l_1(0) < 0$, the 4WS vehicle system undergoes supercritical Hopf bifurcation, as the speed U increases to exceed the critical speed U_c, the stable equilibrium point becomes unstable, and a stable limit cycle is present after the Hopf bifurcation. If $l_1(0) > 0$, the 4WS vehicle system undergoes subcritical Hopf bifurcation, having a unstable limit cycle and stable equilibrium point coexisting before the bifurcation. As the the speed U increases exceeding the critical speed U_c, the stable equilibrium point loses stability and the unstable limit cycle disappears. However, when $l_1(0) = 0$, the 4WS vehicle system may have a degenerate Hopf bifurcation, called Bautin bifurcation, which belongs to codimension-two bifurcations.

3.2 The Bautin bifurcation analysis

Theorem 3.1. *(Bautin) [22] Suppose that a planar system,*

$$\dot{\boldsymbol{x}} = \boldsymbol{f}(\boldsymbol{x}, \boldsymbol{\alpha}), \quad \boldsymbol{x} \in \mathbb{R}^2, \quad \boldsymbol{\alpha} \in \mathbb{R}^2, \tag{3.7}$$

with smooth $\boldsymbol{f}$, has the equilibrium $\boldsymbol{x} = 0$ with eigenvalues

$$\lambda_{1,2} = \mu(\boldsymbol{\alpha}) \pm i\omega(\boldsymbol{\alpha}),$$

for all $\|\boldsymbol{\alpha}\|$ sufficiently small, where $\omega(0) = \omega_0 > 0$. For $\boldsymbol{\alpha} = 0$, let the Bautin bifurcation conditions hold:

$$\mu(0) = 0, and\ l_1(0) = 0,$$

where $l_1(\boldsymbol{\alpha})$ is the first Lyapunov coefficient. Assume that the following genericity conditions are satisfied:
(B_1) *$l_2(0) \neq 0$, where $l_2(0)$ is the second Lyapunov coefficient;*
(B_2) *the map $\boldsymbol{\alpha} \longmapsto (\mu(\boldsymbol{\alpha}), l_1(\boldsymbol{\alpha}))^T$ is regular at $\boldsymbol{\alpha} = 0$.*
Then, by the introduction of a complex variable, applying smooth invertible coordinate transformations that depend smoothly on the parameters, and performing smooth parameter and time changes, the system (3.7)*can be reduced to the complex form*

$$\dot{z} = (\beta_1 + i)z + \beta_2 z|z|^2 + sz|z|^4 + O(|z|^6), \tag{3.8}$$

where $s = \mathrm{sign}(l_2(0)) = \pm 1$.

Set $s=-1$ and rewrite system (3.8) without the $O(|z|^6)$ terms in polar coordinates (ρ,φ), where $z=\rho^{i\varphi}$,

$$\begin{cases} \dot{\rho}=\rho(\beta_1+\beta_2\rho^2-\rho^4), \\ \dot{\varphi}=1, \end{cases} \tag{3.9}$$

where $\beta_1=\frac{\mu(U,a)}{\omega(U,a)},\beta_2=\frac{l_1(U,a)}{\sqrt{|l_2(\boldsymbol{\alpha}(\mu))|}},T=\{(\beta_1,\beta_2):\beta_2^2+4\beta_1=0,\beta_2>0\}$. The bifurcation diagram of system (3.9) is shown in Fig. 2.

Following reference [22] and according to the symmetry of the vehicle system (3.3), the second Lyapunov coefficient $l_2(0)$ is calculated by the formula,

$$l_2(0)=\frac{1}{12\omega_0}Re(\langle \boldsymbol{p},\boldsymbol{E}(\boldsymbol{q},\boldsymbol{q},\boldsymbol{q},\bar{\boldsymbol{q}},\bar{\boldsymbol{q}})+\boldsymbol{C}(\bar{\boldsymbol{q}},\bar{\boldsymbol{q}},h_{30})+3\boldsymbol{C}(\boldsymbol{q},\boldsymbol{q},\bar{h}_{21})+6\boldsymbol{C}(\boldsymbol{q},\bar{\boldsymbol{q}},h_{21})\rangle), \tag{3.10}$$

where

$$h_{30}=(3i\omega_0\boldsymbol{I}-\boldsymbol{A})^{-1}\boldsymbol{C}(\boldsymbol{q},\boldsymbol{q},\boldsymbol{q}),\ \textit{and}\ h_{21}=(i\omega_0\boldsymbol{I}-\boldsymbol{A})^{-1}[\boldsymbol{C}(\boldsymbol{q},\boldsymbol{q},\bar{\boldsymbol{q}})-\langle \boldsymbol{p},\boldsymbol{C}(\boldsymbol{q},\boldsymbol{q},\bar{\boldsymbol{q}})\rangle\boldsymbol{q}].$$

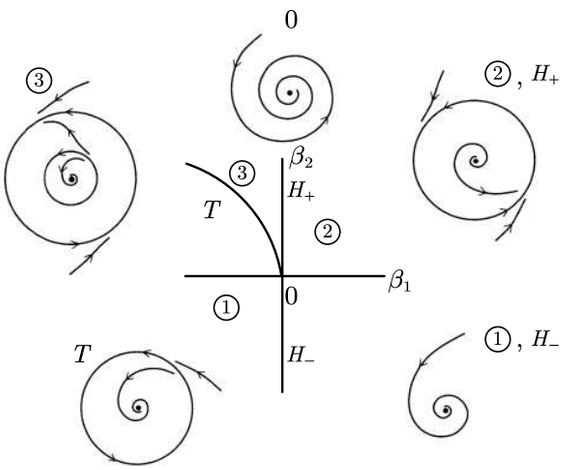

Fig. 2 Bautin bifurcation for $s=-1$.

4 Numerical results, analysis and discussions

4.1 Numerical analysis of stability and Hopf bifurcation

Take the parameters as shown in Table 1, which are given in [8] . Taking the critical speed as the evaluation index, the linear stability boundary in the three-dimensional space is shown in Fig. 3. At those surfaces, the Jacobian matrix $\boldsymbol{A}(U_c)$ has a pair of purely imaginary eigenvalues $\lambda_{1,2}=\pm i\omega$. Below the values of U of the stability boundary surface, the 4WS vehicle system is

Table 1: Values of parameters

Parameter	Comments	Value
m	Mass of the vehicle	1830kg
I_z	Inertia moment of the vehicle body about vertical axis	$2500\text{kg}\cdot\text{m}^2$
a	Distance from the center of gravity of the vehicle to front axles	1.2m
b	Distance from the center of gravity of the vehicle to rear axles	1.4m
T_r	Driver's perceptual time delay	0.2s
L_d	Frontal visibility of the driver	15m
K	Loop gain in the driver model	0.02
K_L	Control strategy coefficient	0.5
U	Vehicle forward speed	–
C_1	Cornering stiffness coefficients	44400N/rad
C_3	Cornering stiffness coefficients	44400N/rad
D_1	Cornering stiffness coefficients	43600N/rad
D_3	Cornering stiffness coefficients	43600N/rad

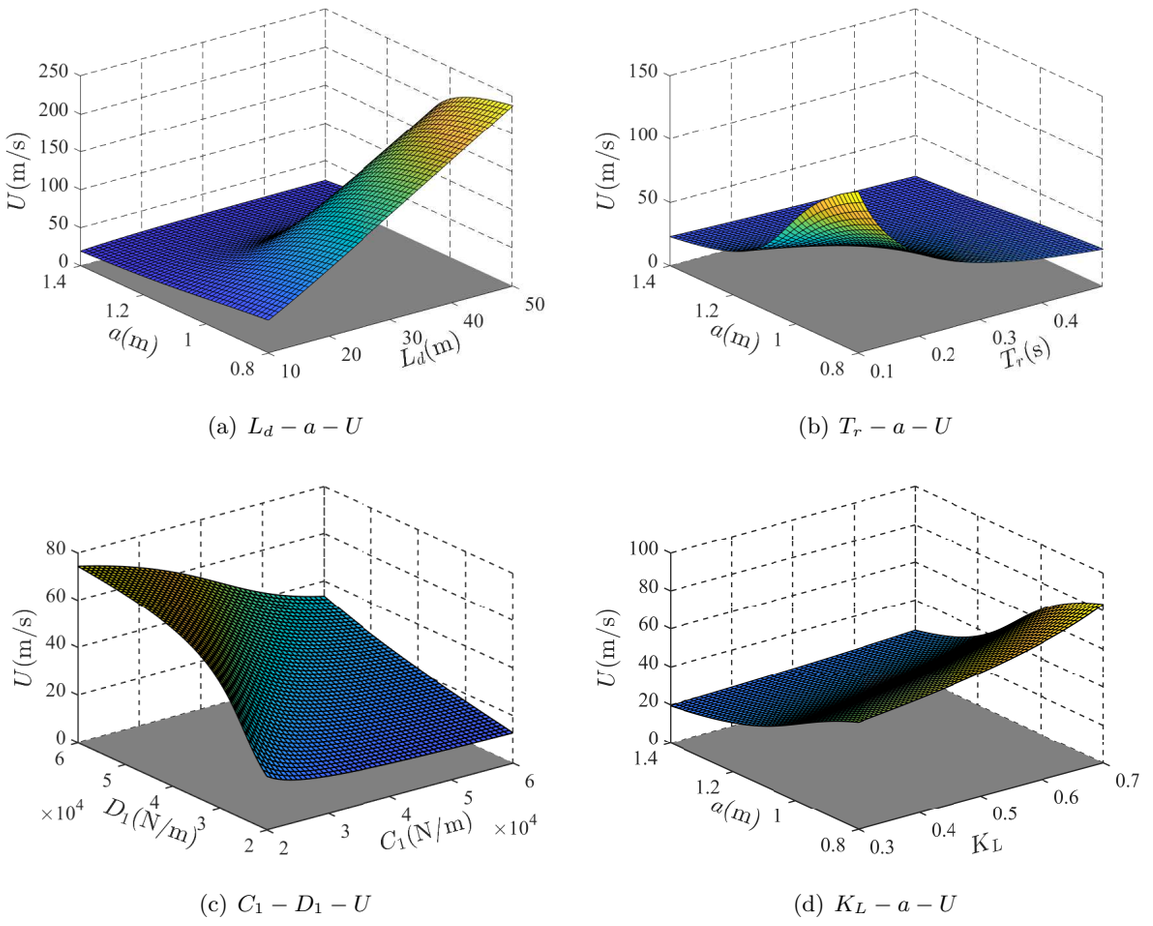

(a) $L_d - a - U$ (b) $T_r - a - U$

(c) $C_1 - D_1 - U$ (d) $K_L - a - U$

Fig. 3 Linear stability surface

stable under moderate perturbations. However, the system is unstable above the surface values of U.

Take the speed U as the control parameter and the other parameters kept fixed as shown in Table 1. The critical speed U_c at the Hopf bifurcation point, calculated by $\Delta_4(U_c) = 0$,

is $U_c = 29.4915$m/s. $\left.\frac{d\Delta_4(U)}{dU}\right|_{U=U_c} = -3.7803 \times 10^5 \neq 0$, which means that the transversality condition is held. The Jacobian matrix at the critical speed is

$$\boldsymbol{A}(U_c) = \begin{bmatrix} -3.2611 & -29.2039 & 0 & 0 & 72.3497 \\ 0.2105 & -4.0525 & 0 & 0 & 18.2080 \\ 1 & 0 & 0 & 29.4915 & 0 \\ 0 & 1 & 0 & 0 & 0 \\ -0.0508 & 0 & -0.1000 & -1.5000 & -5 \end{bmatrix}.$$

The corresponding eigenvalues are

$$\lambda_1 = 1.5752i, \lambda_2 = -1.5752i, \lambda_3 = -4.6007 + 2.7068i, \lambda_4 = -4.6007 - 2.7068i, and\ \lambda_5 = -3.1122.$$

The normalized eigenvectors satisfying Eq. (3.5) are

$$\boldsymbol{p} = \begin{bmatrix} -2.5056 - 2.7050i \\ -0.0730 + 1.1124i \\ -0.8492 - 11.6307i \\ 0.7062 + 0.0464i \\ -0.0835 + 0.2725i \end{bmatrix}, \boldsymbol{q} = \begin{bmatrix} -2.5056 - 2.7050i \\ -0.0730 + 1.1124i \\ -0.8492 - 11.6307i \\ 0.7062 + 0.0464i \\ -0.0835 + 0.2725i \end{bmatrix},$$

and

$$\boldsymbol{C}(\boldsymbol{q}, \boldsymbol{q}, \bar{\boldsymbol{q}}) = \begin{bmatrix} -0.5509 - 20.6272i \\ 1.4577 - 3.6873i \\ -6.4996 + 0.8457i \\ 0.0000 + 0.0000i \\ 0.3306 - 0.0430i \end{bmatrix}.$$

By Eq. (3.6), we calculate the first Lyapunov coefficient as

$$l_1(0) = \frac{1}{2\omega_0} Re(\langle \boldsymbol{p}, \boldsymbol{C}(\boldsymbol{q}, \boldsymbol{q}, \bar{\boldsymbol{q}}) \rangle) = -0.0209 < 0.$$

Therefore, the 4WS vehicle system (2.7) undergoes a supercritical Hopf bifurcation, the trivial equilibrium bifurcates into a limit cycle via the supercritical Hopf bifurcation for $U > U_c$.

The Hopf bifurcation diagram is shown in Fig. 4, where the solid red line represents stable equilibrium point, dashed red line represents unstable equilibrium point, and solid blue line represents the amplitude of limit cycle. If the speed of the 4WS vehicle system is lower than the critical speed U_c, the equilibrium of the system is stable. As the speed of the vehicle system increases exceeding the critical speed U_c, the equilibrium of the system loses stability and bifurcates into a stable limit cycle. And the amplitude of the limit cycle increases as the 4WS vehicle speed increases.

Figure 5 shows the time history of the vehicle system movement at different speeds. It aims to better understanding the Hopf bifurcation process of the system (2.7), where Fig. 5(a) is at 29m/s , below of the critical speed U_c, Fig. 5(b) is at $U = 29.4915$m/s , about the critical speed, and Fig. 5(c) is at 29.52m/s, above the critical speed. It is shown that, when the speed is lower than the critical speed, the system converges to a stable equilibrium position. It means the motion of the 4WS vehicle system will always return to the center line of the road under an initial perturbation. While if the speed is higher than the critical speed, the system converges to a stable periodic motion, which means the vehicle oscillate with a constant amplitude. It indicates that a supercritical Hopf bifurcation occurs in the 4WS vehicle system.

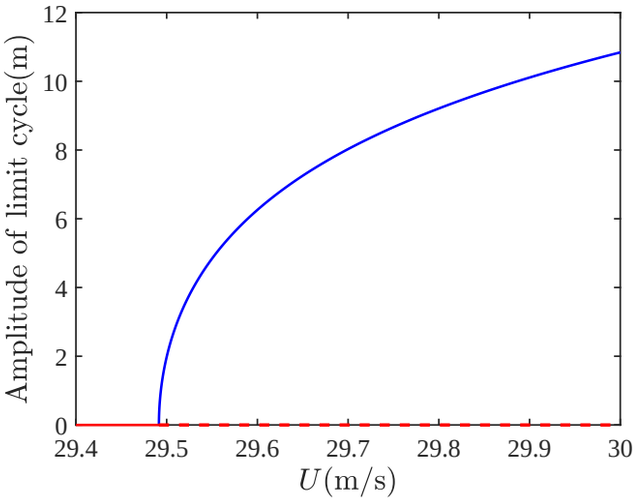

Fig. 4 Supercritical Hopf bifurcation of the 4WS vehicle system (2.7)

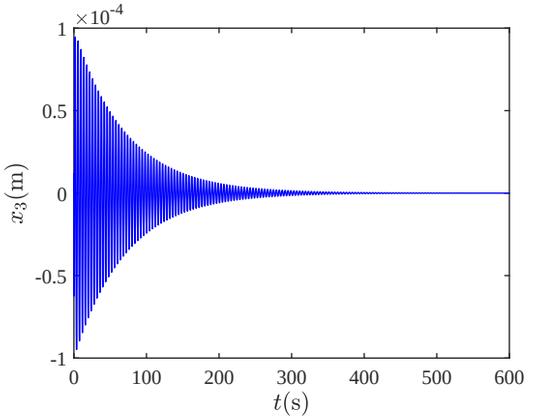

(a) $U = 29$m/s

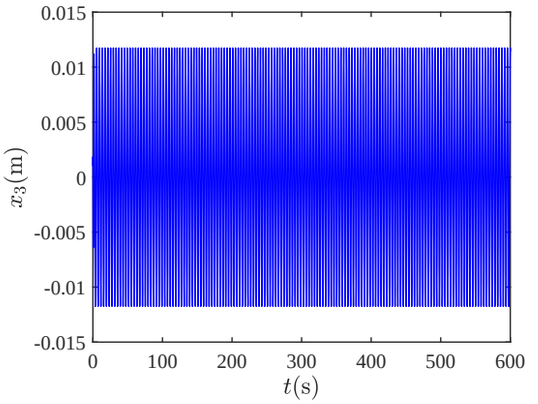

(b) $U = 29.4915$m/s

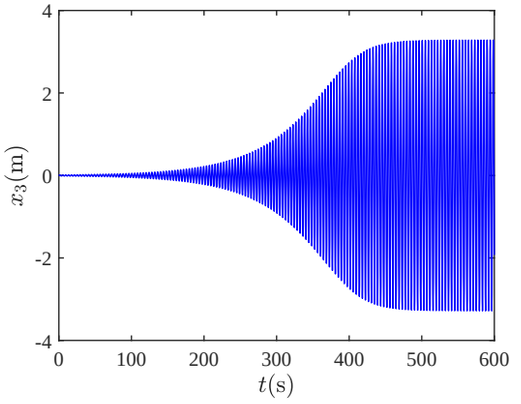

(c) $U = 29.52$m/s

Fig. 5 Time history diagram of the system motion at different speeds

4.2 Effect of system parameters

In this section, the effect of the system parameters on the Hopf bifurcation is analyzed. Fig. 6 shows the effect of different parameters of the system on the Hopf bifurcation point, the type of Hopf bifurcation and the amplitude of the limit cycle. Where dashed red lines represent the amplitude of the unstable limit cycle and solid blue lines represent the amplitude of the stable limit cycle. The points at each line intersects the horizontal coordinate represent the critical speed of the Hopf bifurcation. It can be seen that when the first Lyapunov coefficient $l_1(0) < 0$, a supercritical Hopf bifurcation is present in the system by numerical simulation, while, if the first Lyapunov coefficient $l_1(0) > 0$, a subcritical Hopf bifurcation is present in the system by numerical simulation, validating the theoretical analysis. From Fig. 3 and Fig. 6, we see that with the increase of the frontal visibility distance of the driver L_d, control strategy coefficient K_L and cornering stiffness coefficients of the rear wheels D_1, the critical speed increases. Nevertheless, the critical speed decreases with the increase of the distance from the center of gravity of the vehicle to the front axles a, Driver's perceptual time delay T_r, and cornering stiffness coefficients of the front wheels C_1.

The effect of single and two parameters on the first Lyapunov coefficient $l_1(0)$ are shown in Fig. 7 and Fig. 8, respectively. It is shown that the first Lyapunov coefficient $l_1(0)$ does not change the sign with the increase of control strategy coefficient K_L and Driver's perceptual time delay T_r within a certain range. It means that the type of Hopf bifurcation is unchanged, which can be verified from the Fig. 6(b) and Fig. 6(c). However, the first Lyapunov coefficient changes from a positive to a negative value with the increase of the distance from the center of gravity of the vehicle to the front axles a, and cornering stiffness coefficients of the front wheels C_1. In other words, the subcritical Hopf bifurcation transforms into a supercritical Hopf bifurcation of the 4WS vehicle system, which can be verified from Fig. 6(a) and Fig. 6(e). With the increase of control strategy coefficient K_L, and cornering stiffness coefficients of the rear wheels D_1, the first Lyapunov coefficient changes from a negative to a positive value, and the 4WS vehicle system transitions from supercritical Hopf bifurcation to subcritical Hopf bifurcation, which can be verified from Fig. 6(d) and Fig. 6(f). The influence of two parameters on the first Lyapunov coefficient $l_1(0)$ is depicted in Fig. 8.

4.3 Numerical analysis of the Bautin bifurcation

In this Section, a numerical analysis of the Bautin bifurcation is performed. The forward speed U and the distance from the center of gravity of the vehicle to the front axles a of the 4WS vehicle system are taken as control parameters, and the other parameters are kept fixed as shown in Table 1.

As discussed in the previous section, the sign of the first Lyapunov coefficient $l_1(0)$ may change as the system parameters changes. When the first Lyapunov coefficient $l_1(0)$ changes from positive to negative value, the vehicle system transforms from subcritical Hopf bifurcation into supercritical Hopf bifurcation, and vice-versa, the system transitions from supercritical Hopf

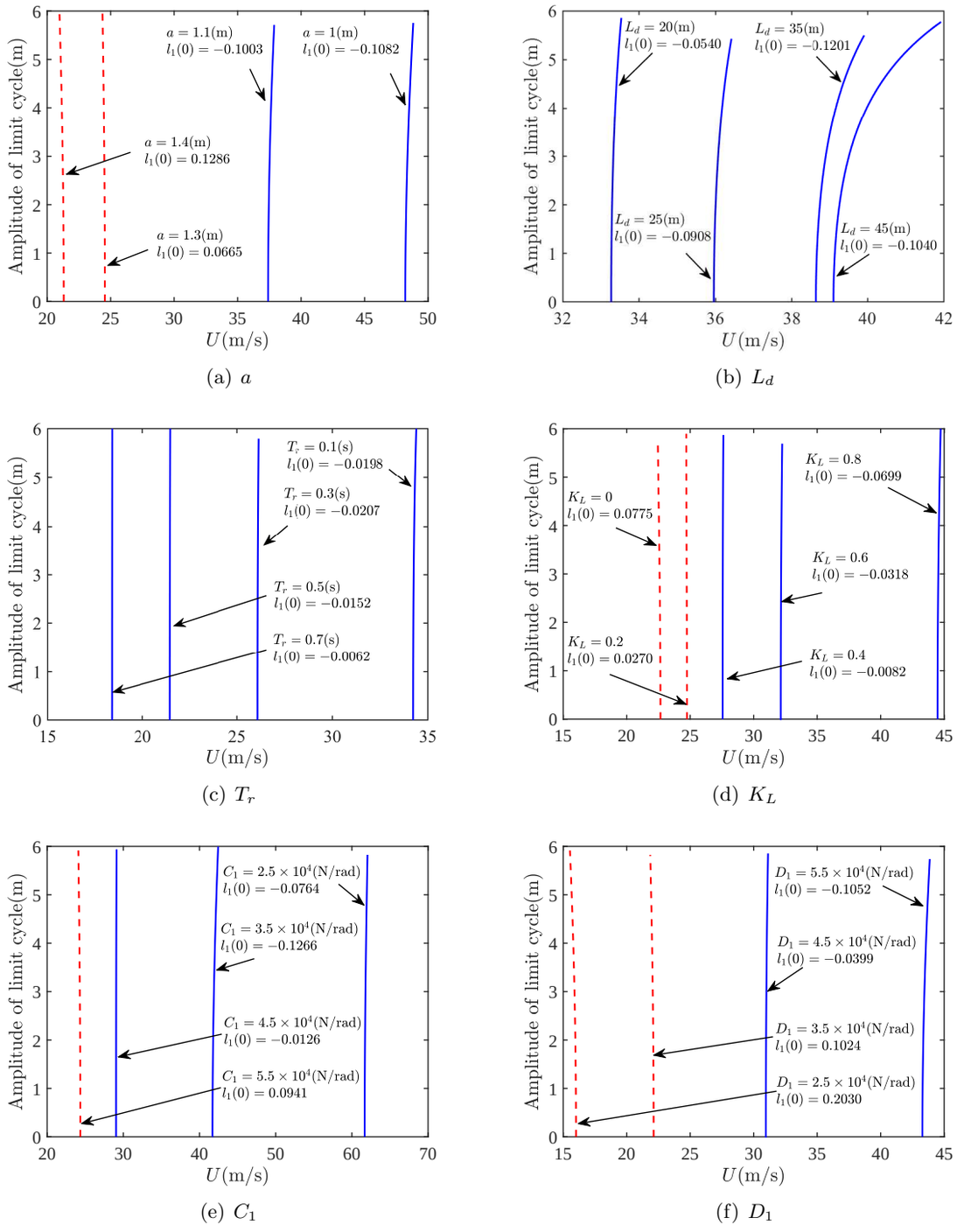

Fig. 6 Effect of the system parameters on the Hopf bifurcation

bifurcation to subcritical Hopf bifurcation. When the sign of the first Lyapunov coefficient $l_1(0)$ changes, it crosses the zero point. If the first Lyapunov coefficient $l_1(0)$ is equal to 0, the 4WS vehicle system may undergoes the Bautin bifurcation. Since the 4WS vehicle system is five dimensional system, the analytical expressions for the critical parameters could not be obtained. Therefore, it is necessary to use numerical calculation methods to determine the

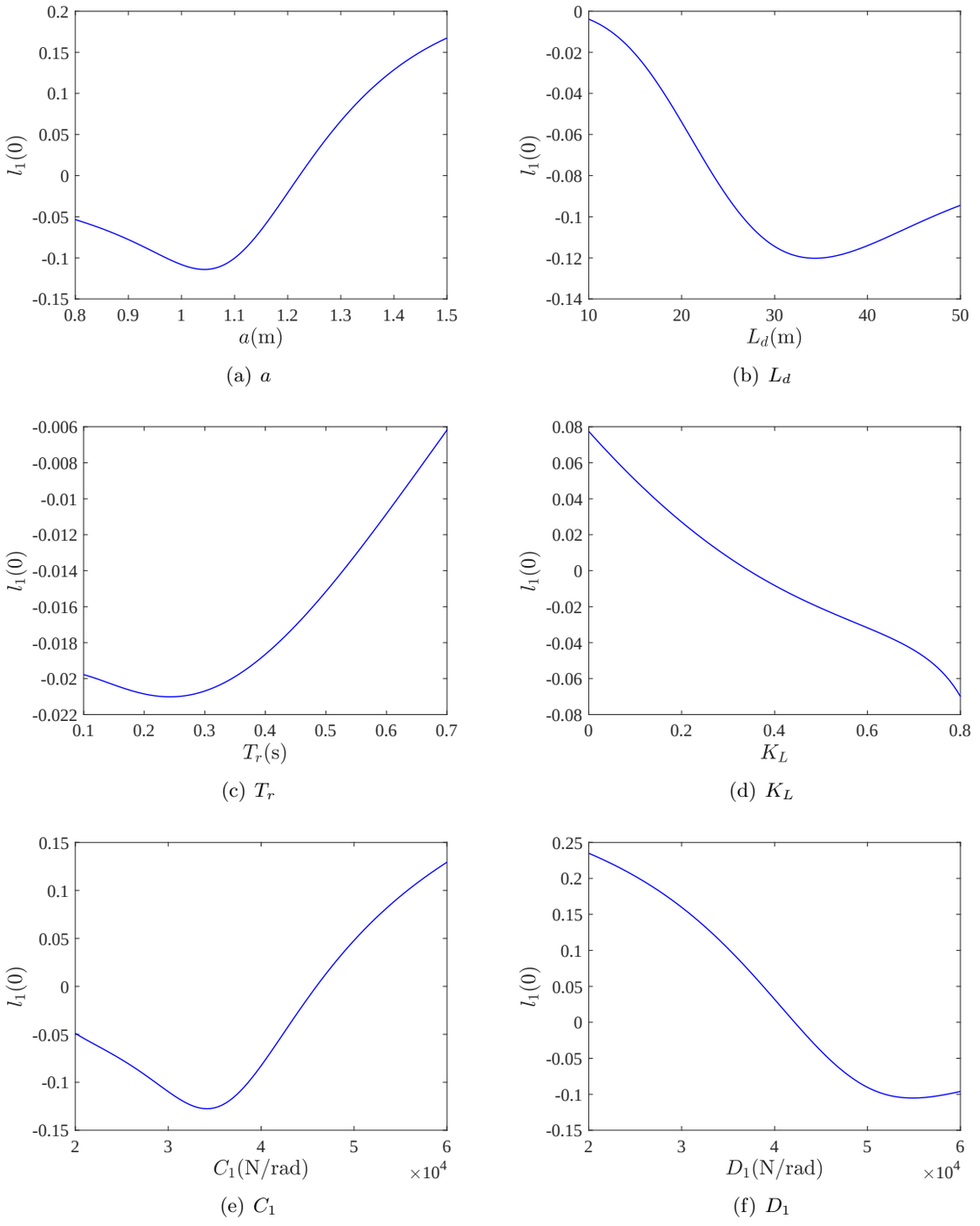

(a) a (b) L_d (c) T_r (d) K_L (e) C_1 (f) D_1

Fig. 7 Effect of single parameter on the first Lyapunov coefficient $l_1(0)$

critical parameters. By equation $\Delta_4(U_c) = 0$ and the formula for the calculation of the first Lyapunov coefficient in Eq. (3.6), the relationship between the a, U and $l_1(0)$ is obtained as shown in the Fig. 9. The plane in Fig. 9 represents $l_1(0) = 0$ and the intersection of the curve with the plane indicates the values of the critical parameters, which can be computed numerically by bisection method as $a_c = 1.2222$m, and $U_c = 28.1860$m/s. At the critical values, by a simple

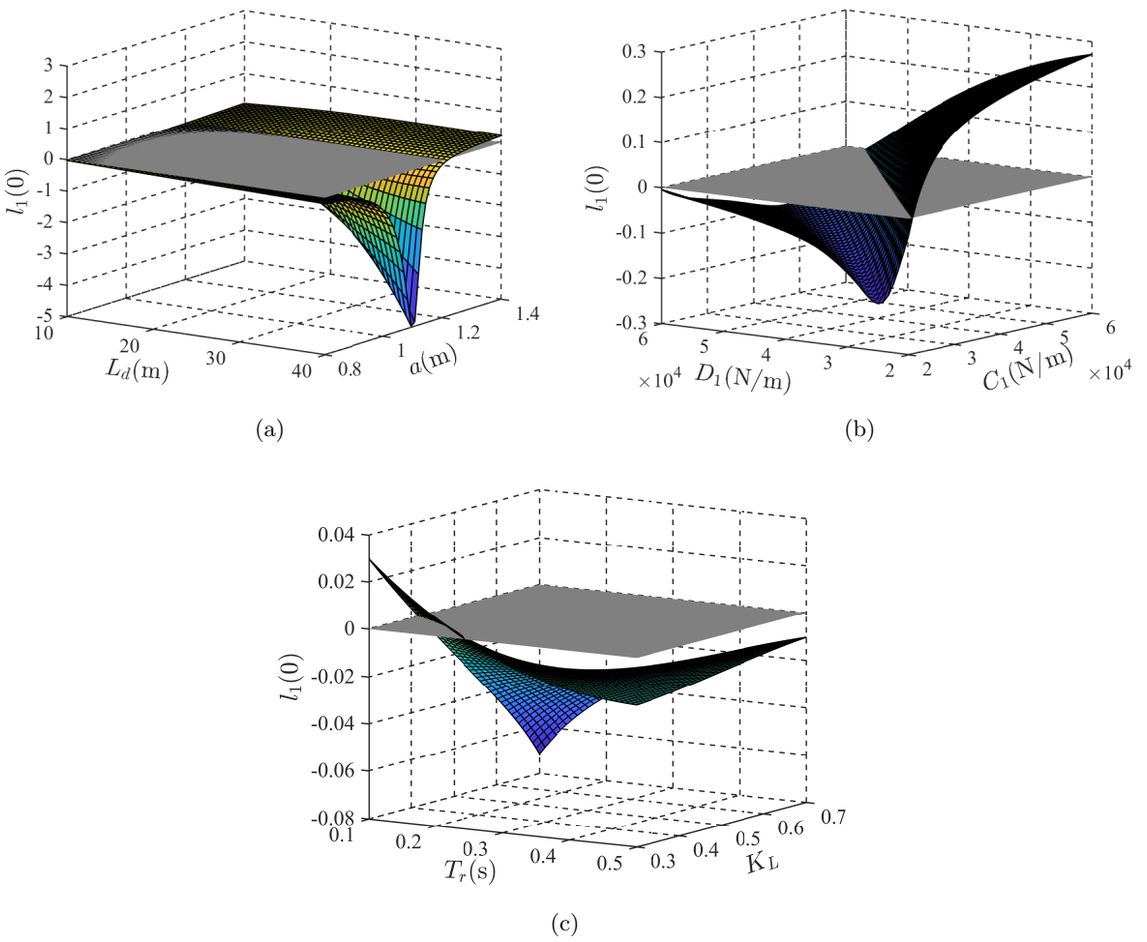

Fig. 8 Effect of two parameters on the first Lyapunov coefficient $l_1(0)$

calculation, we obtain $\lambda_{1,2} = \pm 1.5902$ and $l_2(0) = -0.0640$. By numerical computation, it yields

$$\text{detA} = \begin{pmatrix} \frac{\partial \mu}{\partial a} & \frac{\partial \mu}{\partial U} \\ \frac{\partial l_1}{\partial a} & \frac{\partial l_1}{\partial U} \end{pmatrix} \Bigg|_{\mu=\mu_c} = -0.0259 \neq 0.$$

Therefore, all conditions of Bautin bifurcation in **Theorem 3.1** are held, which means that the Bautin bifurcation occurs for the 4WS vehicle system. Figure 10 shows the Bautin bifurcation diagram of the 4WS vehicle system. Since $l_2(0) = -0.0640 < 0$, so the topological structure of the Bautin bifurcation diagram for the 4WS vehicle system corresponds to the case shown in Fig. 2. The line H corresponds to the Hopf bifurcation curve, H_+ and H_- correspond to a Hopf bifurcation with positive and negative first Lyapunov coefficients, respectively. If a point in the parameter plane crosses H_- from region 1 to region 2, the vehicle system undergoes a supercritical Hopf bifurcation, while a subcritical Hopf bifurcation occurs if a point crosses H_+ from region 3 to region 2.

To better understand the Bautin bifurcation diagram of the 4WS vehicle system in the parameter plane (U, a) shown in Fig. 10, start with a point in region 1 in the parameter plane and make an excursion counterclockwise around the Bautin bifurcation point of the vehicle system.

In region 1, the vehicle system has only a stable equilibrium point. Then, the point crosses the Hopf bifurcation boundary H_- to reach region 2, the vehicle system undergoes a supercritical Hopf bifurcation creating a unique stable limit cycle while the equilibrium point loses its stability. When the point crosses the Hopf bifurcation boundary H_+ from region 2 to region 3, the stable limit cycle survives. Simultaneously, the vehicle system undergoes a subcritical Hopf bifurcation creating an extra unstable limit cycle and the equilibrium point regains its stability. The stable and the unstable limit cycles coexist in the region 3 and disappear when the point crosses the curve T. The point eventually returns to region 1, leaving only a stable equilibrium point.

In order to better understand the local dynamics around the Bautin bifurcation point of the 4WS vehicle system, the phase portraits of three pairs of parameters corresponding to three different regions on the parameters plane (U, a) are depicted in Fig. 11. Fig. 11(a) shows a phase portrait when the parameter (U, a) is in the region 1, it can be seen that the vehicle system converges to a stable equilibrium point for an initial perturbation. If the parameter (U, a) is in the region 2, the vehicle system oscillates periodically whose phase portrait is shown in Fig. 11(b). It can be seen from Fig. 11(c) that when the parameter (U, a) is in the region 3, a stable equilibrium point and a stable limit cycle coexist for the vehicle system. The 4WS vehicle system returns to the centerline of the road or oscillates periodically depend on the initial state.

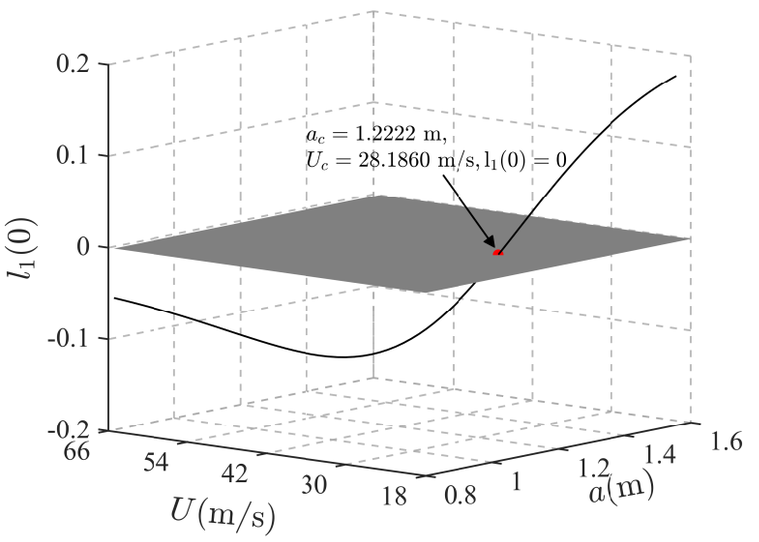

Fig. 9 The relationship of U, a and $l_1(0)$

5 Conclusions

In this work, the stability and Bautin bifurcation of a 4WS vehicle/driver closed-loop system with the nonlinearity from lateral tyre force and geometric relationship are investigated. The application of the bifurcation theory to the 4WS vehicle system allows a prediction of the

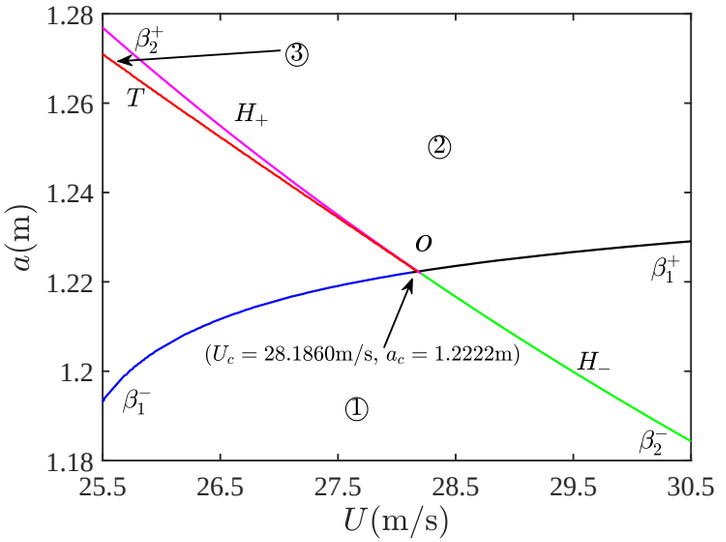

Fig. 10 Bautin bifurcation diagram of the 4WS vehicle system

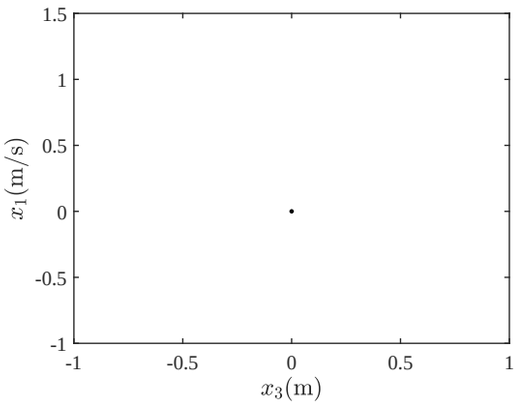

(a) $a = 1.2\text{m}$, $U = 28\text{m/s}$

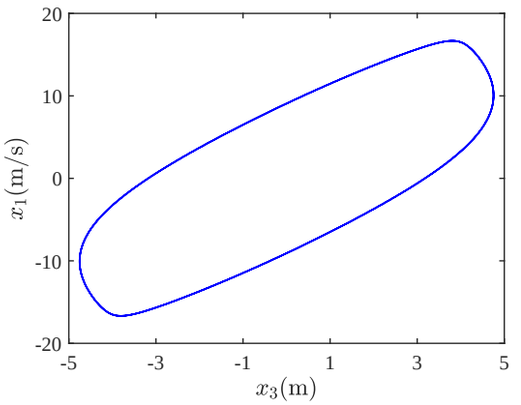

(b) $a = 1.24\text{m}$, $U = 28.5\text{m/s}$

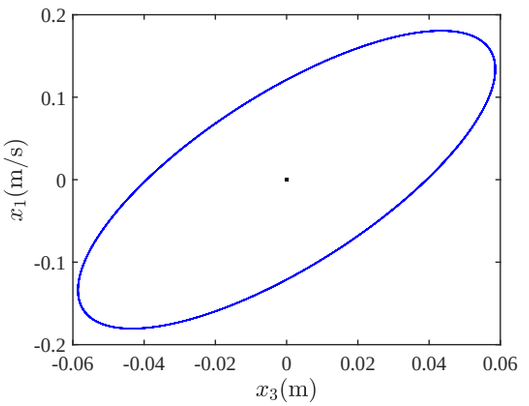

(c) $a = 1.2734\text{m}$, $U = 25.6516\text{m/s}$

Fig. 11 Phase portraits of the 4WS vehicle system in different regions

dynamic behavior for the system beyond linear instability. The centre manifold theory and projection method are used to calculate the first and second Lyapunov coefficients. The first Lyapunov coefficient is used to identify the system undergoing a supercritical or a subcritical Hopf bifurcation. When the first Lyapunov coefficient is equal to zero, the second Lyapunov coefficient is needed for computation in order to better understand the local dynamics of the 4WS vehicle system near the equilibrium.

The forward speed and the distance from the center of gravity of the vehicle to the front axles of the 4WS vehicle system are chosen as the two bifurcation parameters. The Bautin bifurcation diagram of the 4WS vehicle system is plotted in the parameter space to reveals the dynamics of the vehicle system when the control parameters are chosen in different regions. It is shown that the vehicle system convergences to its equilibrium when the parameters are in the region 1 and oscillates periodically when the parameters are in the region 2, while in region 3, the vehicle system returns to its equilibrium for a small system perturbation and oscillates periodically with constant amplitude after a large system perturbation.

The influence of vehicle system parameters on the stability, critical speed, and the type of Hopf bifurcation are also investigated. The results show that with the increase of the frontal visibility distance of the driver control strategy coefficient and the cornering stiffness coefficients of the rear wheels, the critical speed increases. Nevertheless, the critical speed decreases with the increase of the distance from the center of gravity of the vehicle to the front axles, Driver's perceptual time delay, and the cornering stiffness coefficients of the front wheels, which provides a guideline for the vehicle design.

Acknowledgments

This work is supported by the National Natural Science Foundation of China (Nos. 12202168, 12072291,12172306).

Declarations

The authors declare that they have no conflict of interest.

Data availability

The data that support the finding of this study are available from the corresponding author upon reasonable request.

Appendix.

(1) Expression of the matrix $\boldsymbol{A}(\boldsymbol{\mu})$,and the functions $g_i(i=1,\cdots,5)$, $h_i(i=1,\cdots,5)$ in Sect.3.1

$$\boldsymbol{A}(\boldsymbol{\mu})=\begin{bmatrix} -\frac{2(C_1+D_1)}{mU} & -U-\frac{2(aC_1-bD_1)}{mU} & 0 & 0 & \frac{2}{m}(C_1+K_LD_1) \\ -\frac{2(aC_1-bD_1)}{I_zU} & -\frac{2(a^2C_1+b^2D_1)}{I_zU} & 0 & 0 & \frac{2}{I_z}(aC_1-bK_LD_1) \\ 1 & 0 & 0 & U & 0 \\ 0 & 1 & 0 & 0 & 0 \\ -\frac{KL_d}{T_rU} & 0 & -\frac{K}{T_r} & -\frac{KL_d}{T_r} & -\frac{1}{T_r} \end{bmatrix},$$

$$\begin{aligned}
g_1=&\frac{2}{m}\Bigg\{C_1\left[\frac{1}{2}\left(\frac{x_1+ax_2}{U}-x_5\right)x_5^2+\frac{1}{3}\cdot\frac{(x_1+ax_2)^3}{U^3}\right]+C_3\left(\frac{x_1+ax_2}{U}-x_5\right)^3\\
&+D_1\left[\frac{1}{2}\left(\frac{x_1-bx_2}{U}-K_Lx_5\right)K_L^2x_5^2+\frac{1}{3}\cdot\frac{(x_1-bx_2)^3}{U^3}\right]+D_3\left(\frac{x_1-bx_2}{U}-K_Lx_5\right)^3\Bigg\},\\
g_2=&\frac{2}{I_z}\Bigg\{aC_1\left[\frac{1}{2}\left(\frac{x_1+ax_2}{U}-x_5\right)x_5^2+\frac{1}{3}\cdot\frac{(x_1+ax_2)^3}{U^3}\right]+aC_3\left(\frac{x_1+ax_2}{U}-x_5\right)^3\\
&-bD_1\left[\frac{1}{2}\left(\frac{x_1-bx_2}{U}-K_Lx_5\right)K_L^2x_5^2+\frac{1}{3}\cdot\frac{(x_1-bx_2)^3}{U^3}\right]\\
&-bD_3\left(\frac{x_1-bx_2}{U}-K_Lx_5\right)^3\Bigg\},\\
g_3=&-\frac{1}{2}x_1x_4^2-\frac{1}{6}Ux_4^3,\\
g_4=&0,\\
g_5=&\frac{KL_d}{2T_r}\left(\frac{1}{U}x_1x_4^2+\frac{1}{3}x_4^3\right),\\
h_1=&\frac{2}{m}\Bigg\{-\frac{C_1}{5}\cdot\frac{(x_1+ax_2)^5}{U^5}-\frac{C_1}{24}\left(\frac{x_1+ax_2}{U}-x_5\right)x_5^4-C_3\left(\frac{x_1+ax_2}{U}-x_5\right)^2\frac{(x_1+ax_2)^3}{U^3}\\
&-\frac{1}{2}\left[\frac{C_1}{3}\cdot\frac{(x_1+ax_2)^3}{U^3}+C_3\left(\frac{x_1+ax_2}{U}-x_5\right)^3\right]x_5^2\\
&-\frac{D_1}{5}\cdot\frac{(x_1-bx_2)^5}{U^5}-\frac{D_1}{24}\left(\frac{x_1-bx_2}{U}-K_Lx_5\right)K_L^4x_5^4-D_3\left(\frac{x_1-bx_2}{U}-K_Lx_5\right)^2\frac{(x_1-bx_2)^3}{U^3}\\
&-\frac{1}{2}\left[\frac{D_1}{3}\cdot\frac{(x_1-bx_2)^3}{U^3}+D_3\left(\frac{x_1-bx_2}{U}-K_Lx_5\right)^3\right]K_L^2x_5^2\Bigg\},\\
h_2=&\frac{2}{I_z}\Bigg\{-\frac{aC_1}{5}\cdot\frac{(x_1+ax_2)^5}{U^5}-\frac{aC_1}{24}\left(\frac{x_1+ax_2}{U}-x_5\right)x_5^4-aC_3\left(\frac{x_1+ax_2}{U}-x_5\right)^2\frac{(x_1+ax_2)^3}{U^3}\\
&-\frac{a}{2}\left[\frac{C_1}{3}\cdot\frac{(x_1+ax_2)^3}{U^3}+C_3\left(\frac{x_1+ax_2}{U}-x_5\right)^3\right]x_5^2\\
&+\frac{bD_1}{5}\cdot\frac{(x_1-bx_2)^5}{U^5}+\frac{bD_1}{24}\left(\frac{x_1-bx_2}{U}-K_Lx_5\right)K_L^4x_5^4+bD_3\left(\frac{x_1-bx_2}{U}-K_Lx_5\right)^2\frac{(x_1-bx_2)^3}{U^3}\\
&+\frac{b}{2}\left[\frac{D_1}{3}\cdot\frac{(x_1-bx_2)^3}{U^3}+D_3\left(\frac{x_1-bx_2}{U}-K_Lx_5\right)^3\right]K_L^2x_5^2\Bigg\},
\end{aligned}$$

$$
\begin{aligned}
h_3 =& \frac{x_1 x_4^4}{24} + \frac{U x_4^5}{120}, \\
h_4 =& 0, \\
h_5 =& -\frac{KL_d}{24T_r}\left(\frac{x_1 x_4^4}{U} + \frac{x_4^5}{5}\right).
\end{aligned}
$$

(2) Coefficients of characteristic equation for the matrix $\boldsymbol{A(\mu)}$ in Sect.3.1

$$
\begin{aligned}
a_0 =& 1 \\
a_1 =& \frac{1}{T_r} + \frac{2(C_1+D_1)}{mU} + \frac{2(a^2C_1+b^2D_1)}{I_zU}, \\
a_2 =& \frac{2}{T_r mU}[(1+KL_d)C_1 + (1+KK_LL_d)D_1] + \frac{2(a^2C_1+b^2D_1)}{T_rI_zU} + \frac{4L^2C_1D_1}{mI_zU^2} - \frac{2(aC_1-bD_1)}{I_z}, \\
a_3 =& \frac{4LC_1D_1}{T_rI_zmU^2}[L + KL_d(aK_L+b)] + \frac{2K}{T_rm}(C_1+K_LD_1) - \frac{2(aC_1-bD_1)}{T_rI_z}, \\
a_4 =& \frac{4KLC_1D_1}{T_rI_zmU}(aK_L+b) + \frac{4KLL_dC_1D_1}{T_rI_zmU}(1-K_L), \\
a_5 =& \frac{4K(1-K_L)LC_1D_1}{T_rI_zm}.
\end{aligned}
$$

References

[1] T. Gillespie. Fundamentals of Vehicle Dynamics. Warrendale, PA: Society of Automotive Engineers, (1992).

[2] P. C. Miao, D. H. Li, S. Yin, et al. Double grazing bifurcations of the non-smooth railway wheelset systems. Nonlinear Dynamics. 2023, 111: 2093-2110.

[3] S. H. Li, J. Y. Wu, B. Hu. Research on lateral stability, bifurcation and chaotic motions of heavy vehicle with road direction disturbance. Applied Mathematics and Mechanics, 2013, 34(9): 891-899.

[4] Z. Liu, G. Payre, P. Bourassa. Nonlinear oscillations and chaotic motions in a road vehicle system with driver steering control. Nonlinear Dynamics, 1996, 9(3): 281-304.

[5] L. Palkovics. Effect of the controller parameters on the steerability of the four wheel steered car. Vehicle System Dynamics. 1992, 21: 109-128.

[6] Y. H. Cho, J. Kim. Design of optimal four-wheel steering system. Vehicle System Dynamics, 1995, 24: 661-682.

[7] M. Nagai, E. Ueda, A. Moran. Nonlinear design to approach four-wheel-steering system using neural network. Vehicle System Dynamics. 1995, 24: 329-342.

[8] L. Dai, Q. Han. Stability and Hopf bifurcation of a nonlinear model for a four-wheel-steering vehicle system. Communications in Nonlinear Science and Numerical Simulations, 2004, 9(3): 331-341.

[9] H. Y. Hu, Z. Q. Wu. Stability and Hopf bifurcation of four-wheel-steering vehicles involving driver's delay. Nonlinear Dynamics. 2000, 22(4): 361-374.

[10] S. W. Shen, J. Wang, P. Shi, et al. Nonlinear dynamics and stability analysis of vehicle plane motions. Vehicle System Dynamics. 2007, 45(1): 15-35.

[11] V. Nguyen, G. Schultz, B. Balachandran. Lateral load transfer effects on bifurcation behavior of four-wheel vehicle system. Journal of Computational and Nonlinear Dynamics, 2009, 4(4): 1724-1732.

[12] F. D. Rossa. M. Gobbi, G. Mastinu, et al. Bifurcation analysis of a car and driver model. Vehicle System Dynamics, 2014, 52(sup1): 142-156.

[13] H. K. Sa, C. C. Chou. On the stability in the sense of Lyapunov of a rubber tire vehicle. Journal of Dynamics, Measurement, and Control, ASME, 1976, 98(4): 394-394.

[14] D. Schramm, Hiller, M, Bardini,R. Vehicle Dynamics: Modeling and Simulation. Springer, Berlin Heidelberg (2018).

[15] E. Bakker, H. B. Pacejka, L. Lidener. A new tire model with an application in vehicle dynamics studies. Fourth Autotechnologies Conference, Monte Carlo, SAE 890087, 1989. 83-95.

[16] A. Higuchi, Y. Saitoh. Optimal control of four wheel steering vehicle. Vehicle System Dynamics, 1993, 22: 397-410.

[17] S. Tousi, A. K. Bajai, W. Soedel. Closed-loop directional stability of car-trailer combinations in straight-line motion. Vehicle System Dynamics, 1992, 21: 333-360.

[18] K. Guo, H. Guan. Modelling of driver/vehicle directional control system. Vehicle System Dynamics, 1993, 22: 141-184.

[19] C. C. Macadam, G. E. Johnson. Application of elementary neural networks and preview sensors for representing driver steering control behavior. Vehicle System Dynamics1996, 25(1): 3-30.

[20] T. Legouis, A. Laneville, P. Bourassa, et al. Characterization of dynamic vehicle stability using two models of the human pilot behaviour. Vehicle System Dynamics, 1986, 15(1): 1-18.

[21] W. M. Liu. Criterion of Hopf bifurcation whitout using eigenvalues. Journal of Mathematical Analysis and Applications, 1994, 18(2): 250-255.

[22] Y. A. Kuznetsov. Elements of Applied Bifurcation Theory, 3rd edn. Springer, New York (2004).

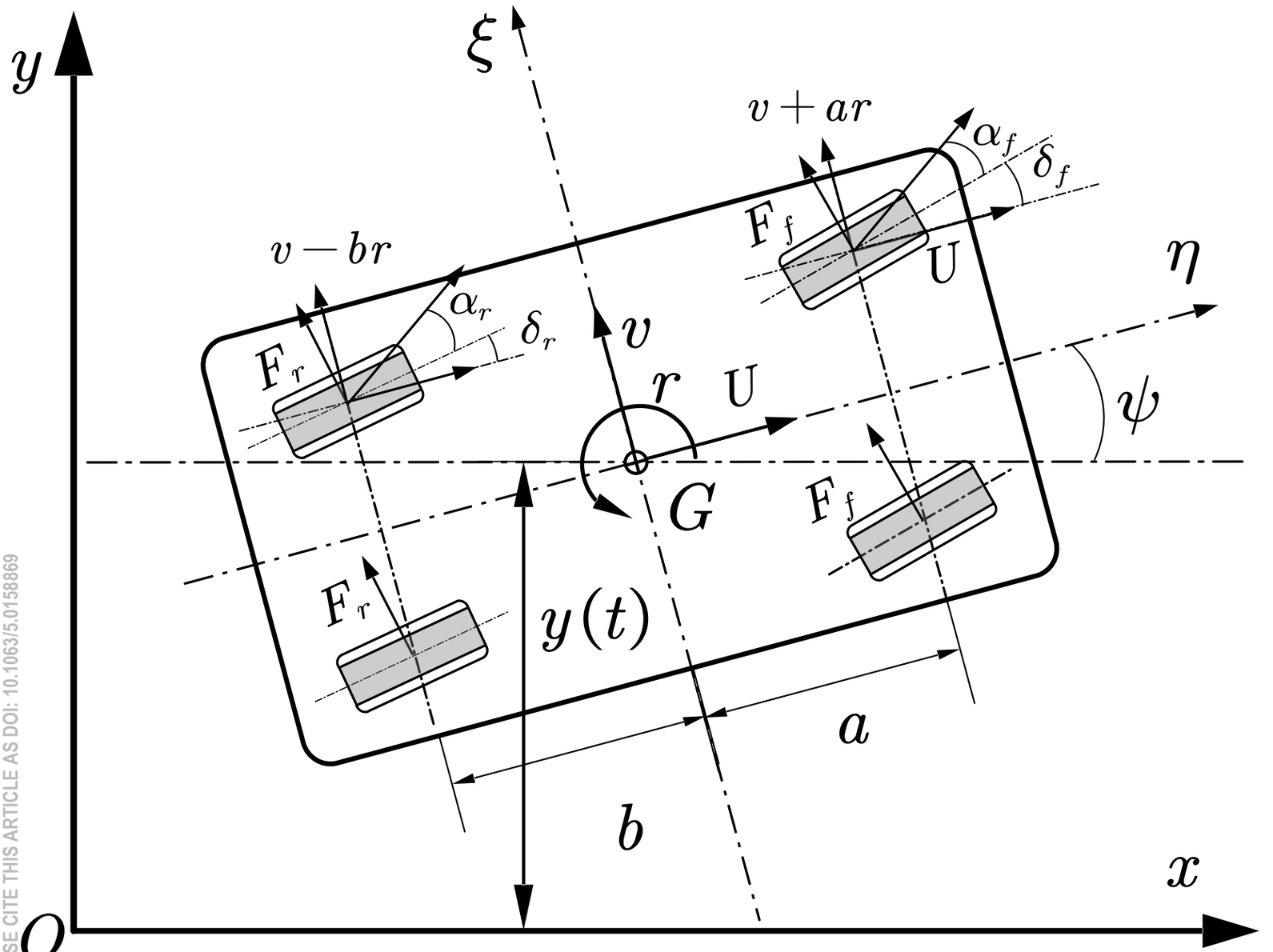

AIP Publishing

Chaos
An Interdisciplinary Journal
of Nonlinear Science

ACCEPTED MANUSCRIPT

PLEASE CITE THIS ARTICLE AS DOI: 10.1063/5.0158869

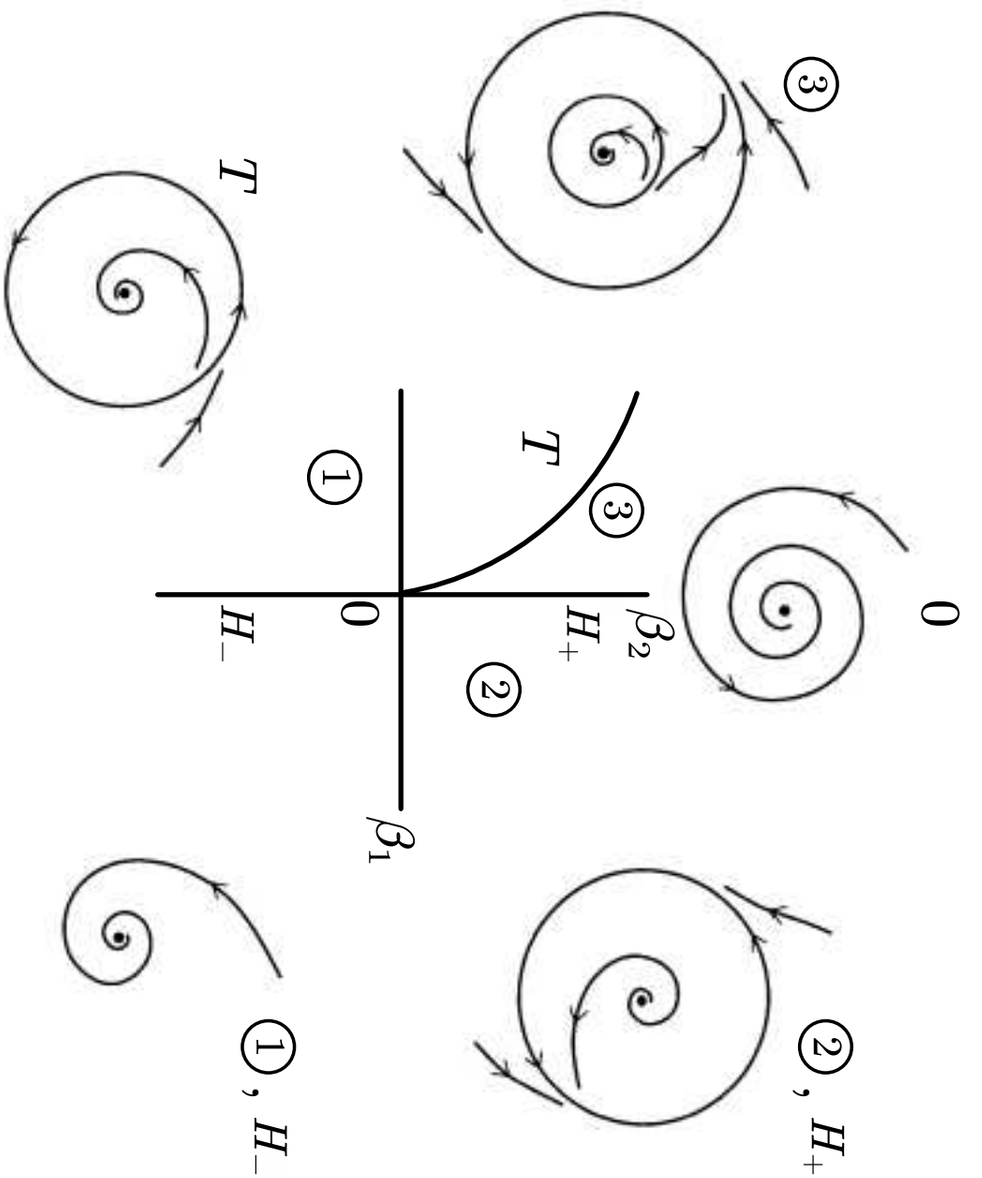

AIP Publishing

Chaos
An Interdisciplinary Journal
of Nonlinear Science

PLEASE CITE THIS ARTICLE AS DOI: 10.1063/5.0158869

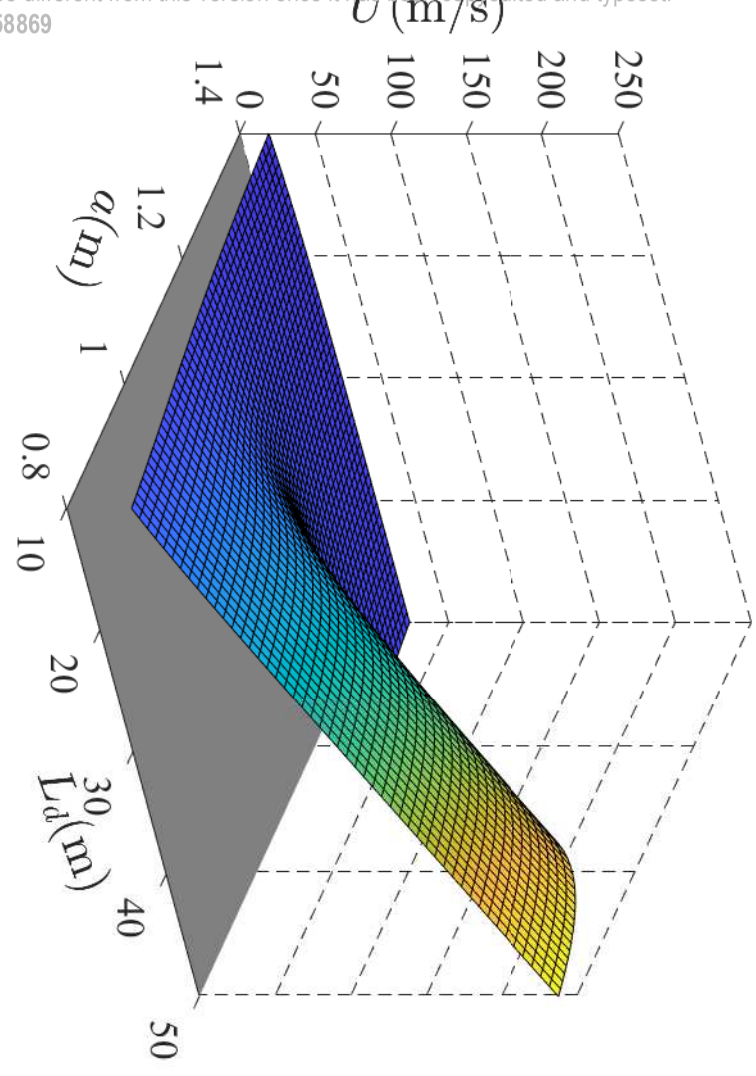

AIP Publishing

Chaos
An Interdisciplinary Journal
of Nonlinear Science

PLEASE CITE THIS ARTICLE AS DOI: 10.1063/5.0158869

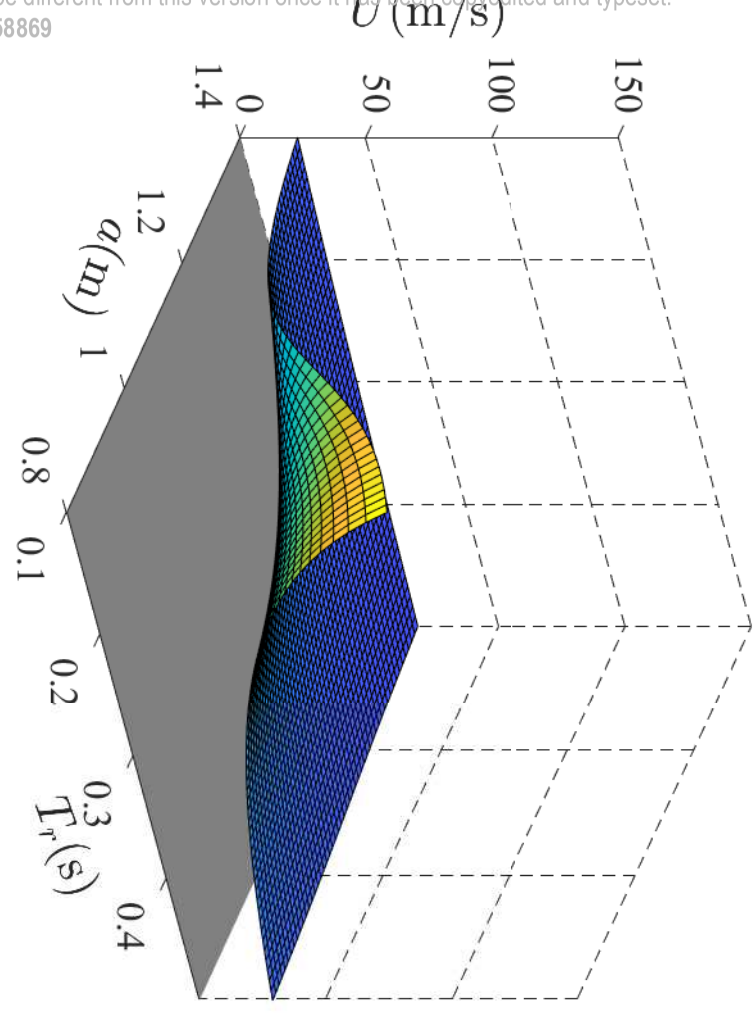

AIP Publishing

Chaos
An Interdisciplinary Journal
of Nonlinear Science

PLEASE CITE THIS ARTICLE AS DOI: 10.1063/5.0158869

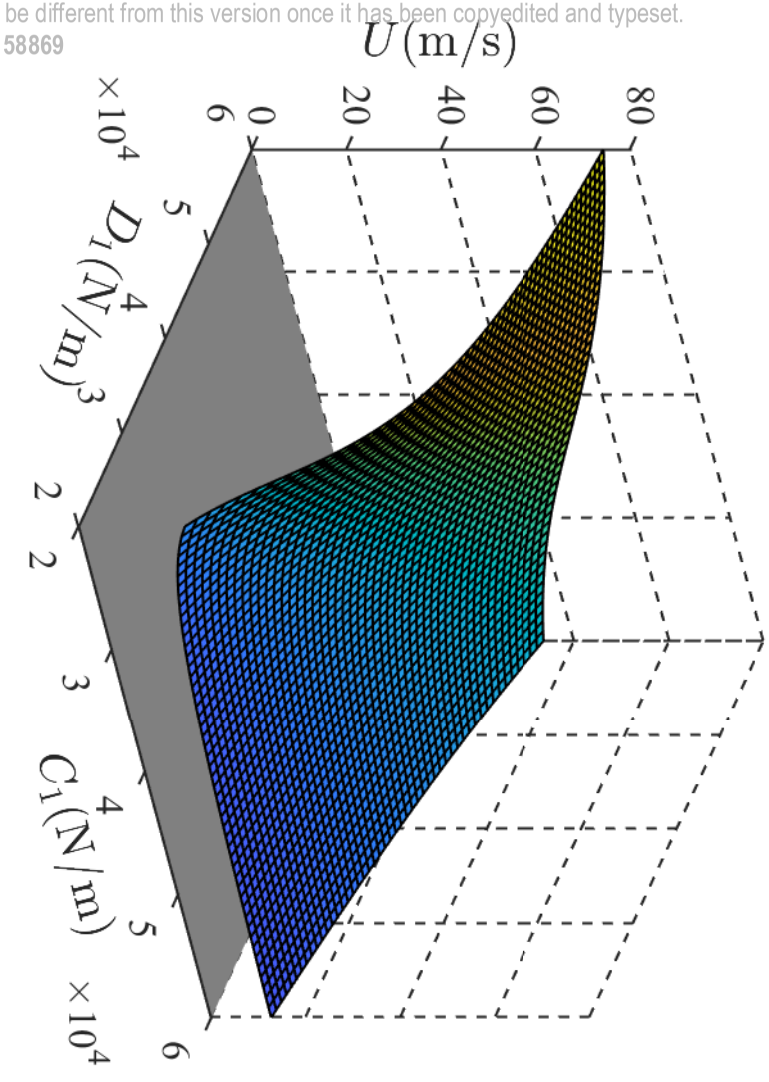

AIP Publishing

Chaos
An Interdisciplinary Journal
of Nonlinear Science

PLEASE CITE THIS ARTICLE AS DOI: 10.1063/5.0158869

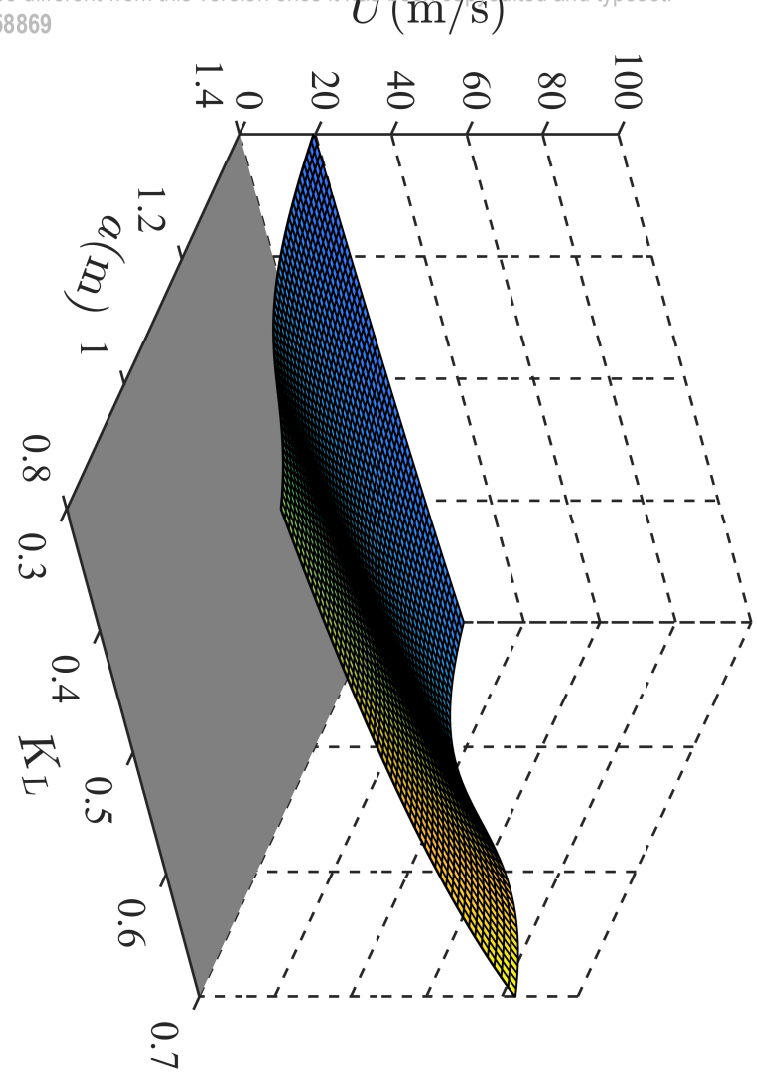

AIP Publishing
Chaos
An Interdisciplinary Journal
of Nonlinear Science

PLEASE CITE THIS ARTICLE AS DOI: 10.1063/5.0158869

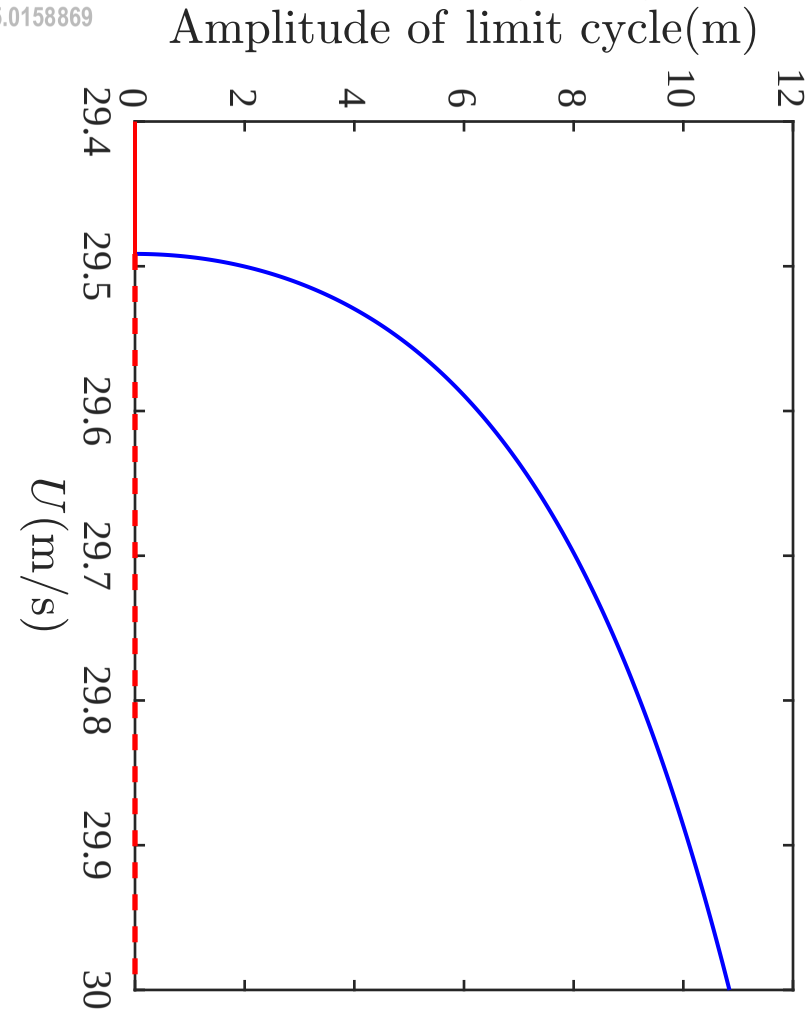

AIP Publishing

Chaos
An Interdisciplinary Journal
of Nonlinear Science

PLEASE CITE THIS ARTICLE AS DOI: 10.1063/5.0158869

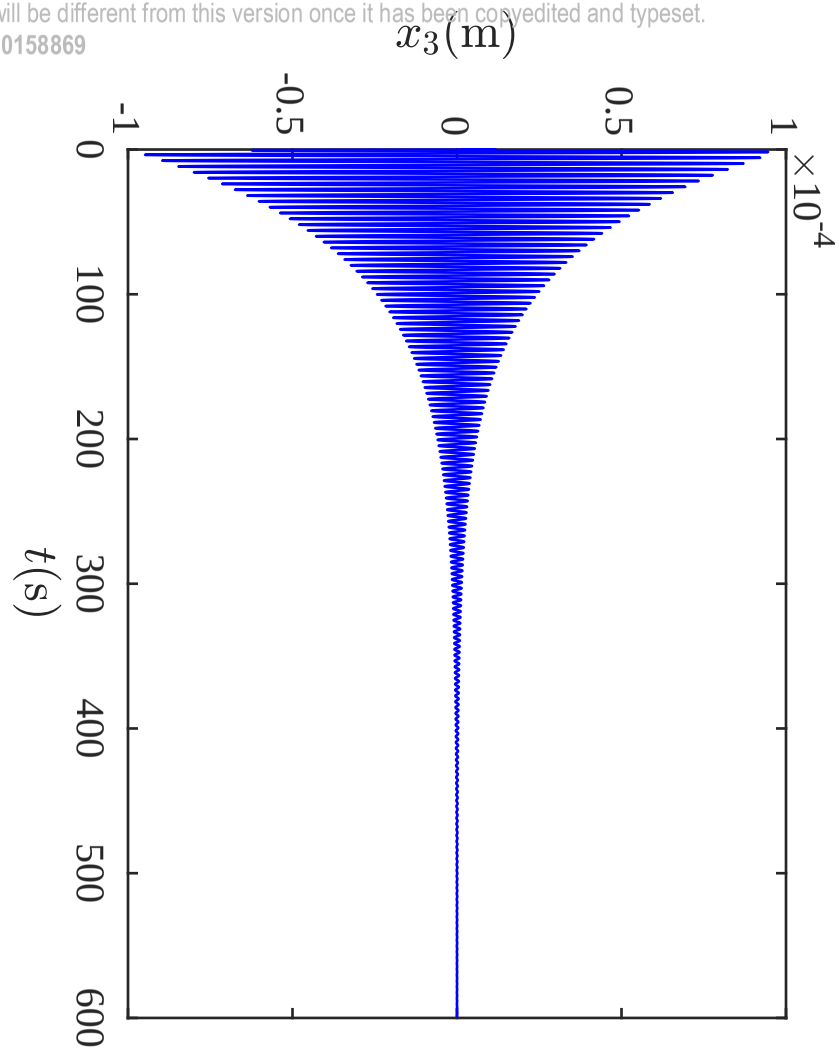

AIP Publishing
Chaos
An Interdisciplinary Journal
of Nonlinear Science

PLEASE CITE THIS ARTICLE AS DOI: 10.1063/5.0158869

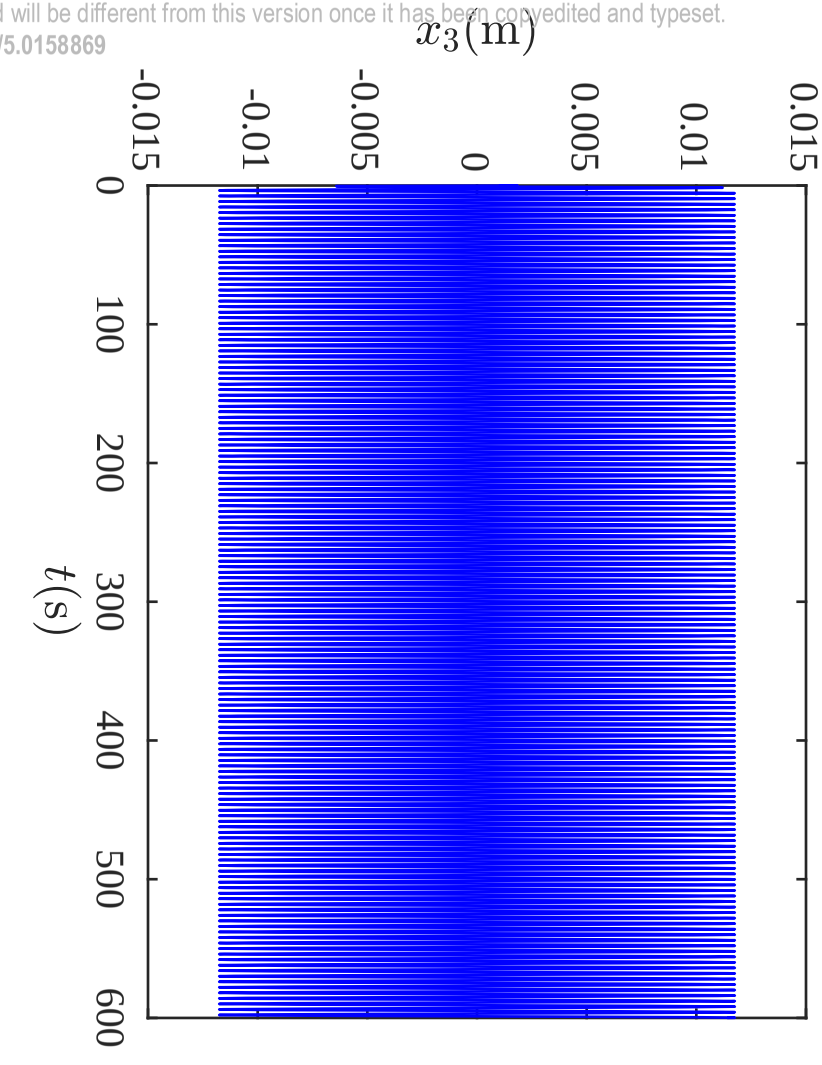

AIP Publishing

Chaos
An Interdisciplinary Journal
of Nonlinear Science

PLEASE CITE THIS ARTICLE AS DOI: 10.1063/5.0158869

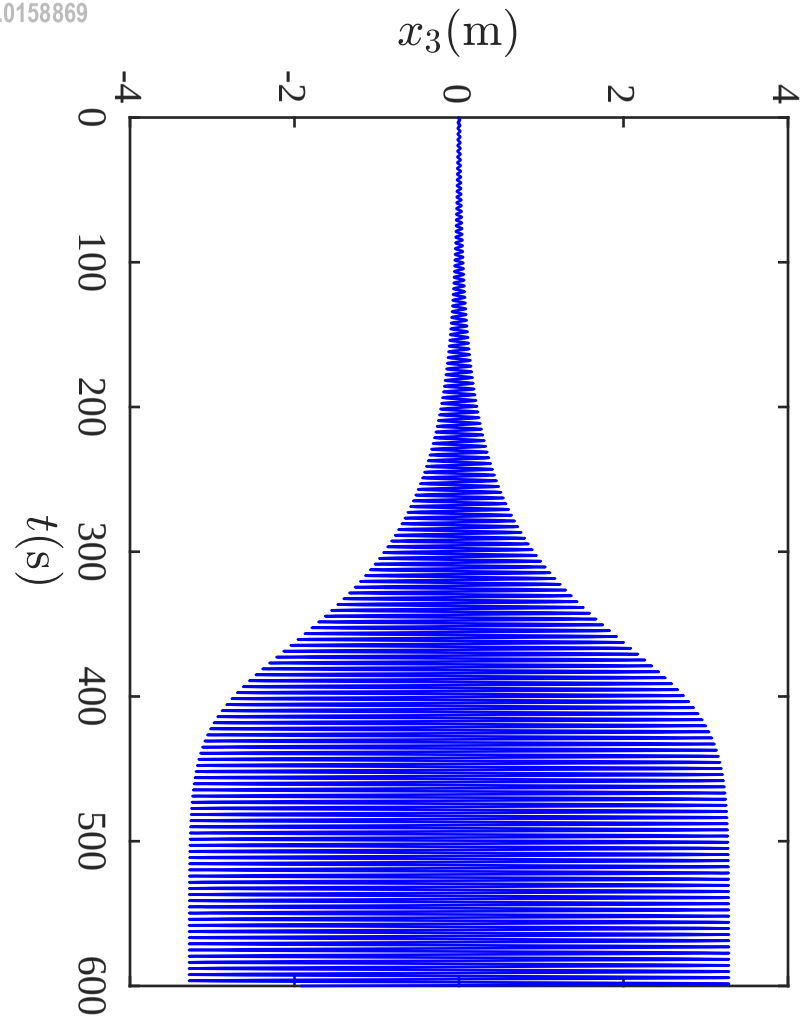

AIP Publishing

Chaos
An Interdisciplinary Journal
of Nonlinear Science

PLEASE CITE THIS ARTICLE AS DOI: 10.1063/5.0158869

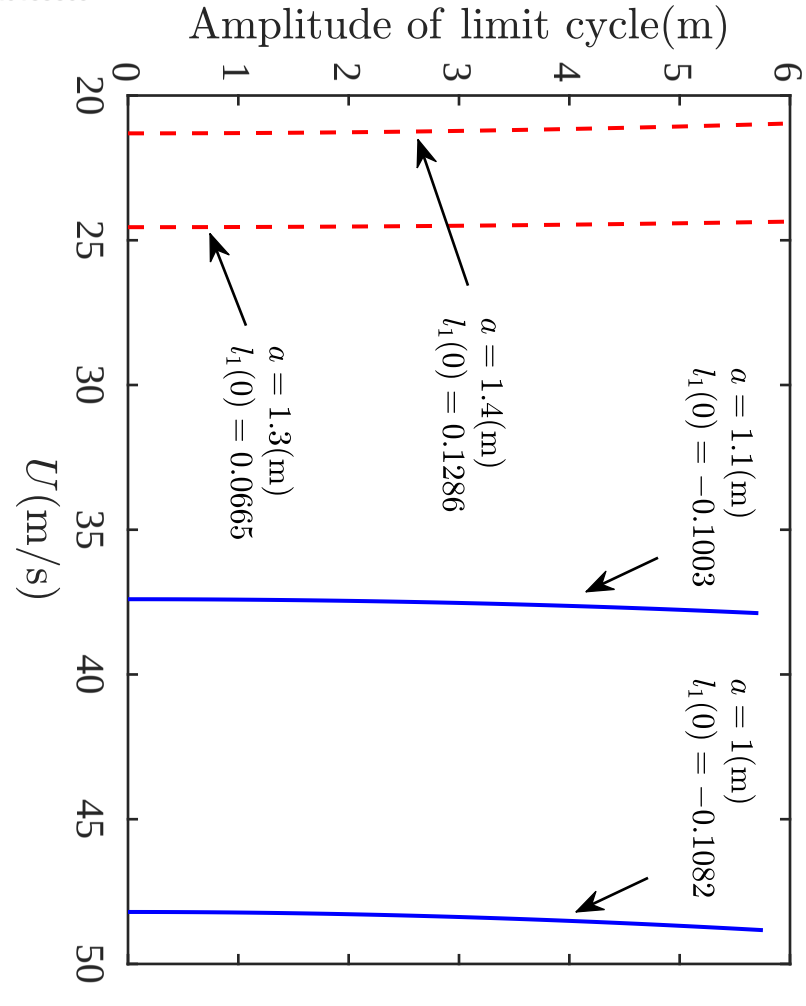

AIP Publishing

Chaos
An Interdisciplinary Journal
of Nonlinear Science

PLEASE CITE THIS ARTICLE AS DOI: 10.1063/5.0158869

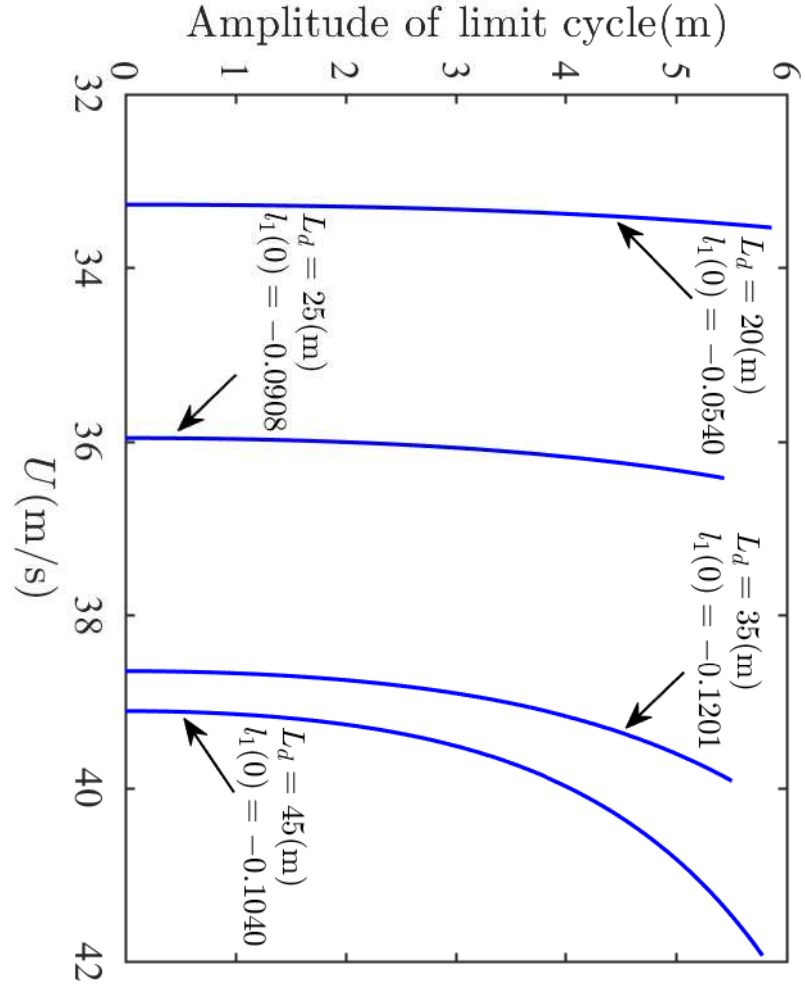

Chaos
An Interdisciplinary Journal
of Nonlinear Science

AIP Publishing

AIP Publishing

Chaos
An Interdisciplinary Journal
of Nonlinear Science

PLEASE CITE THIS ARTICLE AS DOI: 10.1063/5.0158869

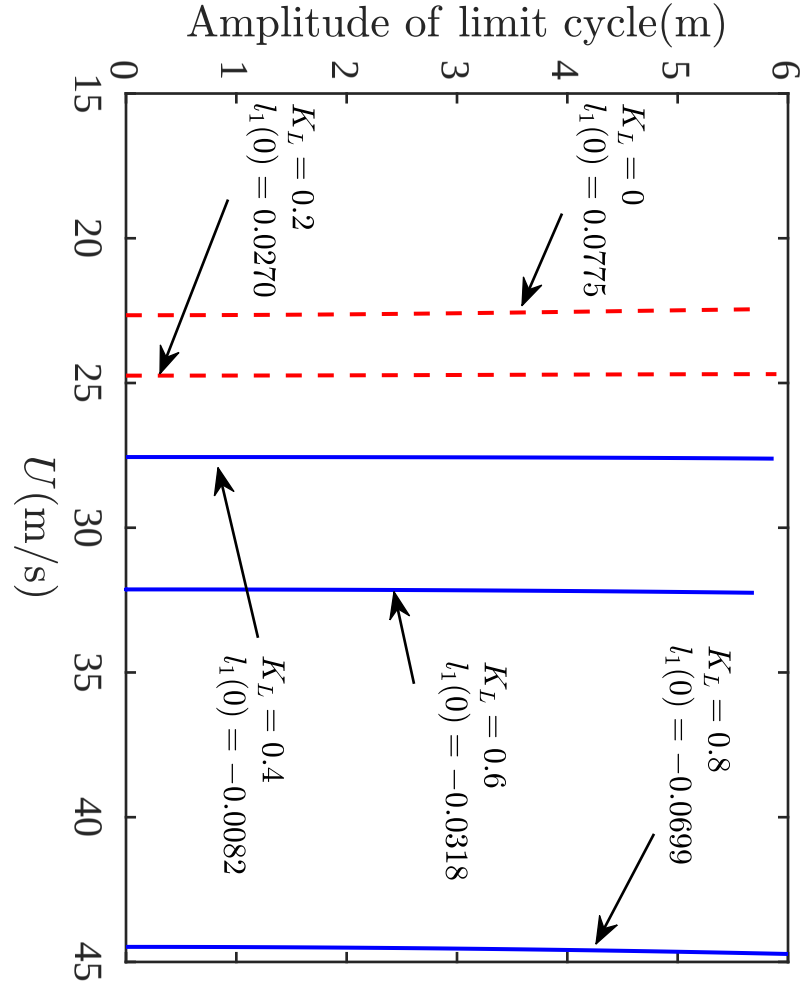

AIP Publishing

Chaos
An Interdisciplinary Journal
of Nonlinear Science

PLEASE CITE THIS ARTICLE AS DOI: 10.1063/5.0158869

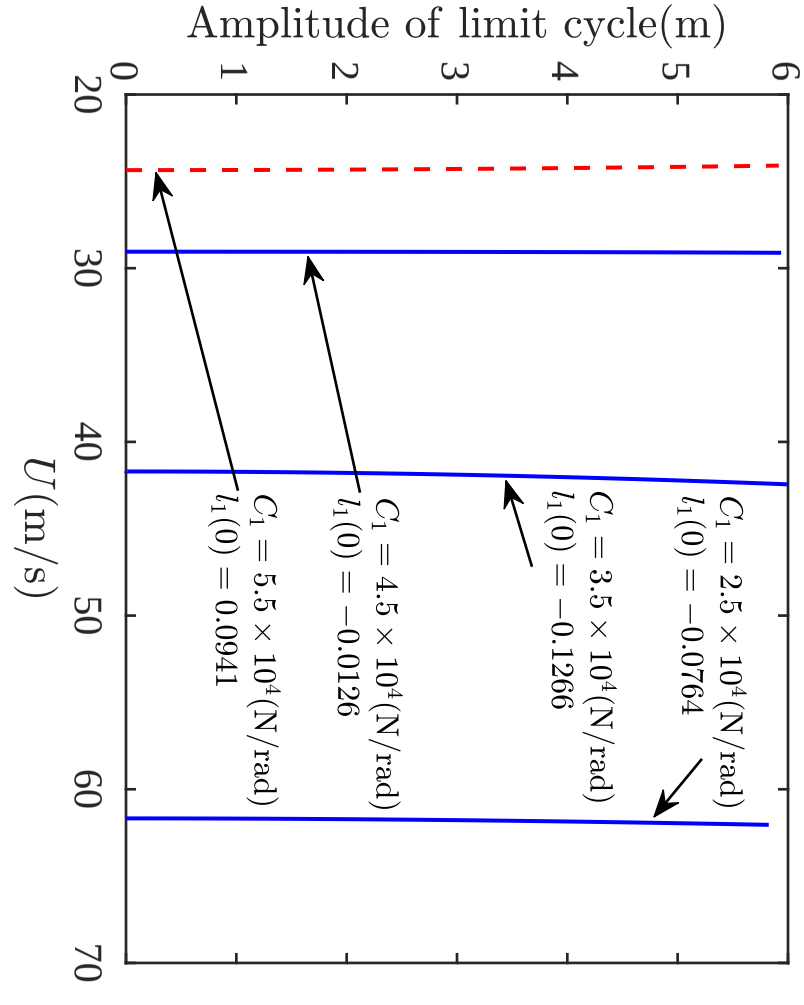

AIP Publishing

Chaos
An Interdisciplinary Journal
of Nonlinear Science

PLEASE CITE THIS ARTICLE AS DOI: 10.1063/5.0158869

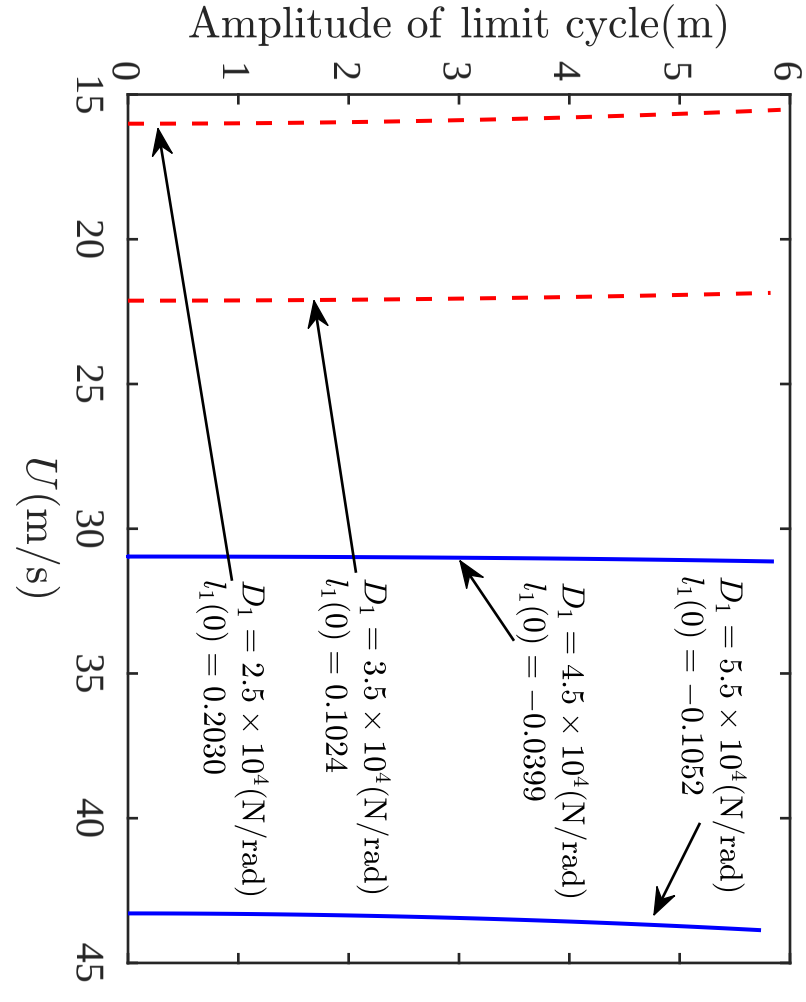

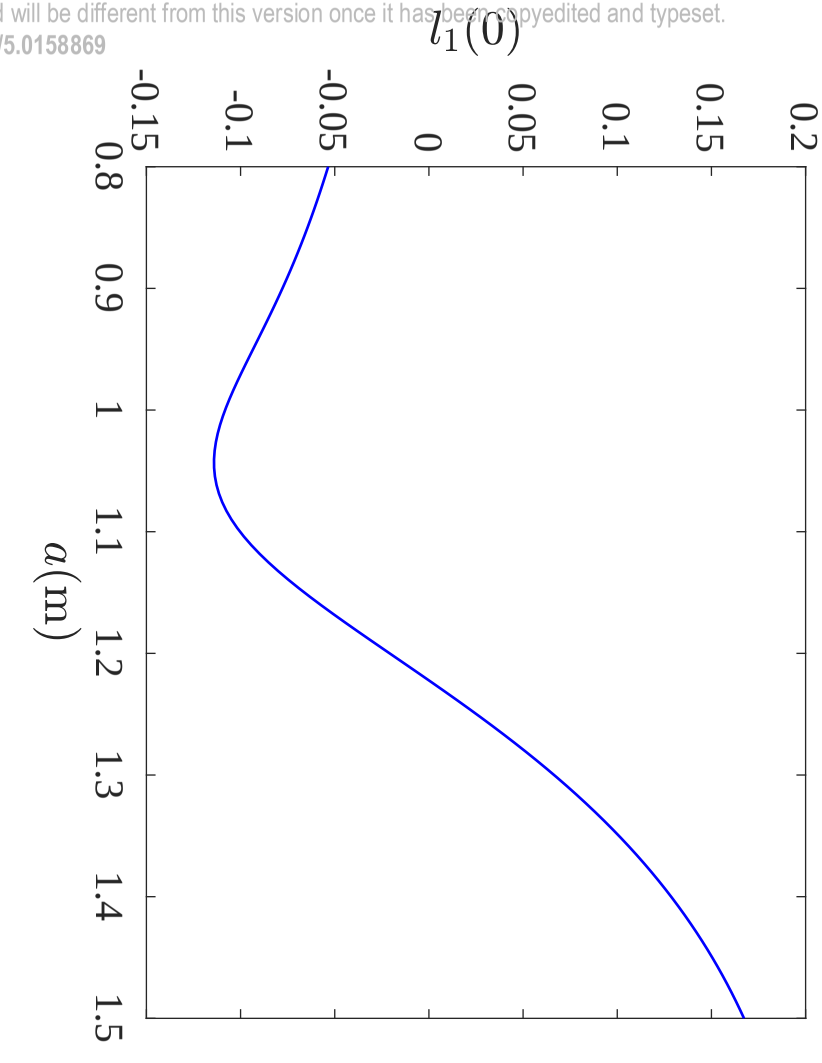

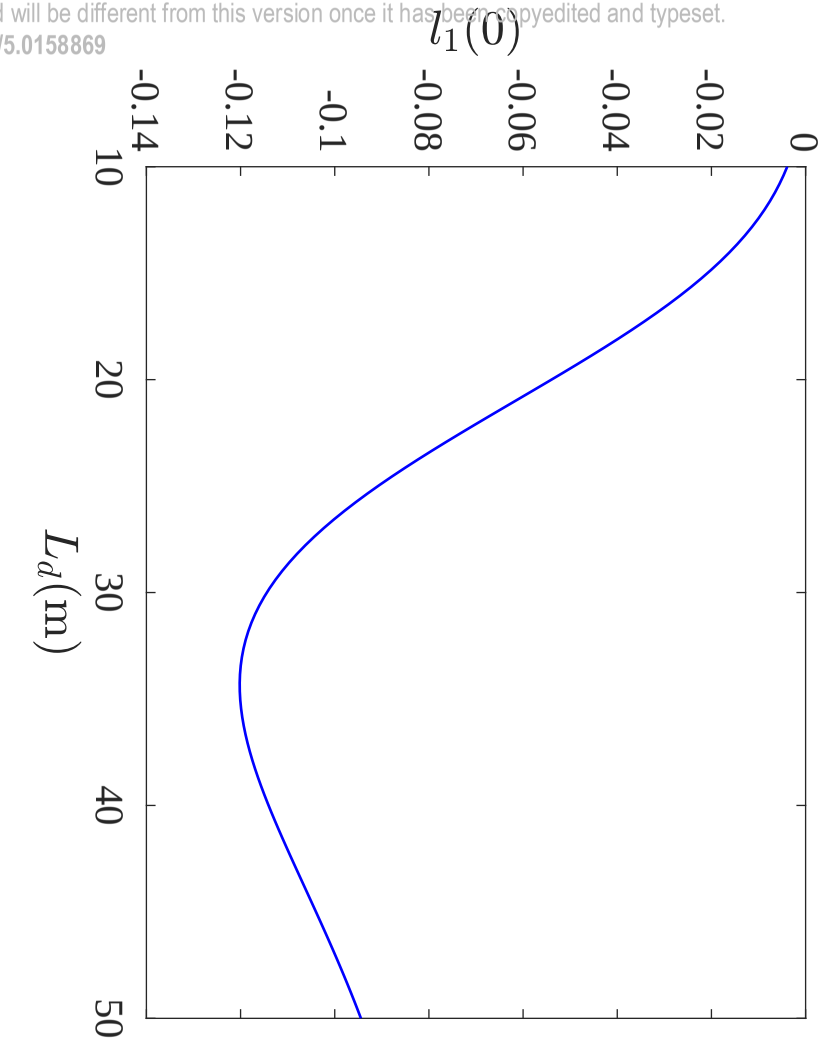

AIP Publishing
Chaos
An Interdisciplinary Journal
of Nonlinear Science

PLEASE CITE THIS ARTICLE AS DOI: 10.1063/5.0158869

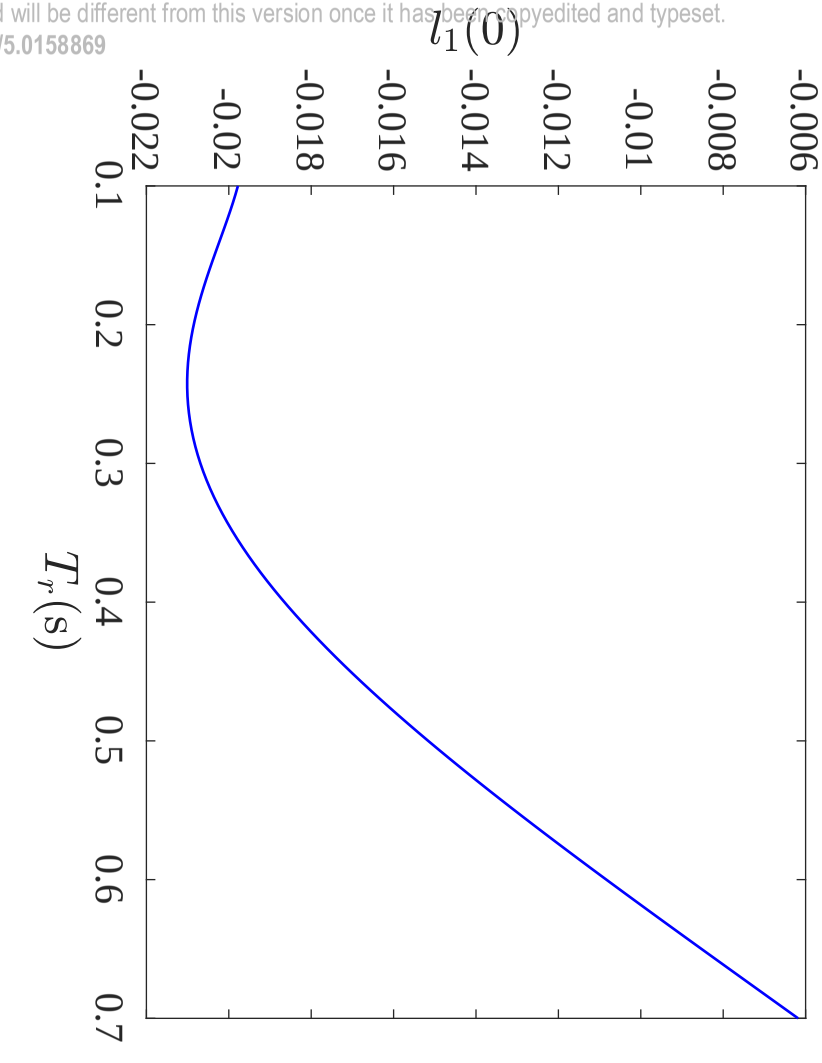

AIP Publishing

Chaos
An Interdisciplinary Journal
of Nonlinear Science

PLEASE CITE THIS ARTICLE AS DOI: 10.1063/5.0158869

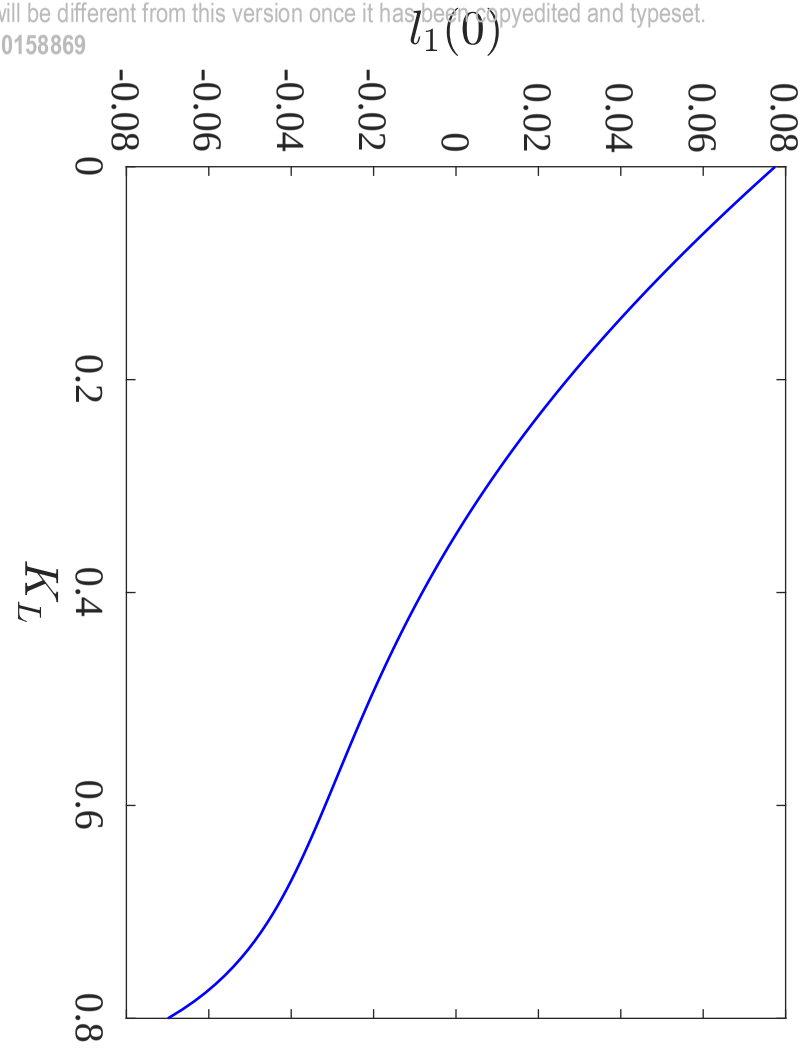

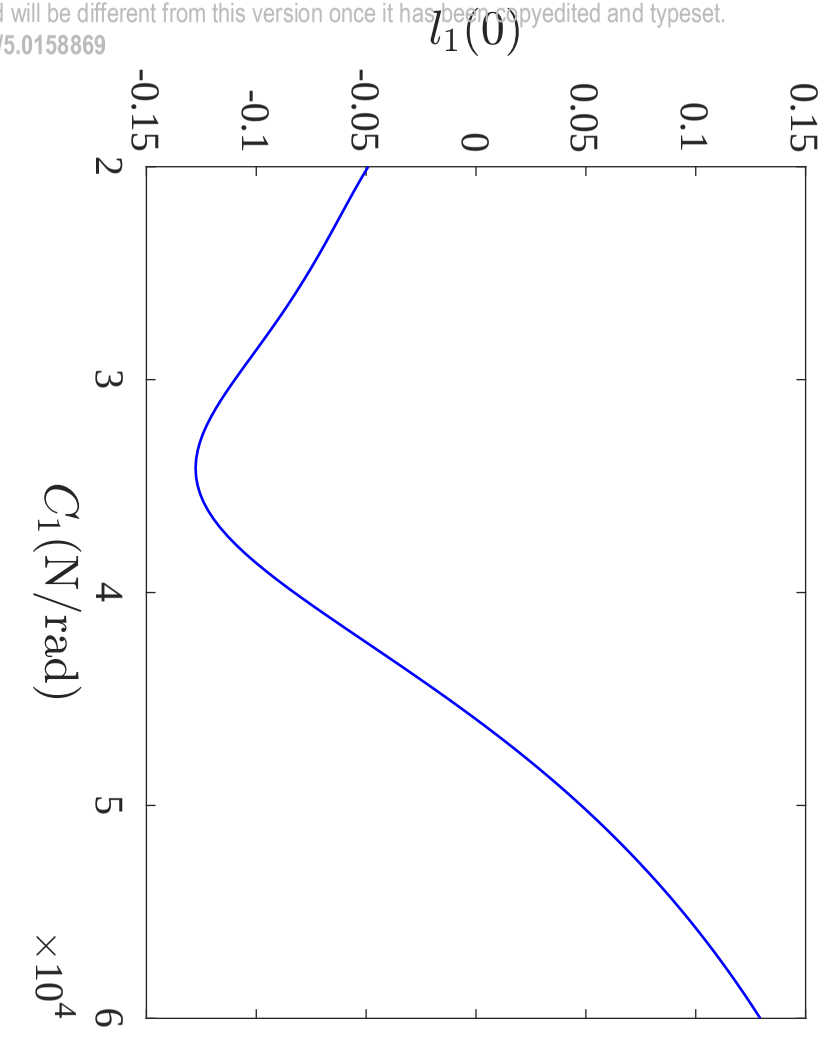

AIP Publishing

Chaos
An Interdisciplinary Journal
of Nonlinear Science

PLEASE CITE THIS ARTICLE AS DOI: 10.1063/5.0158869

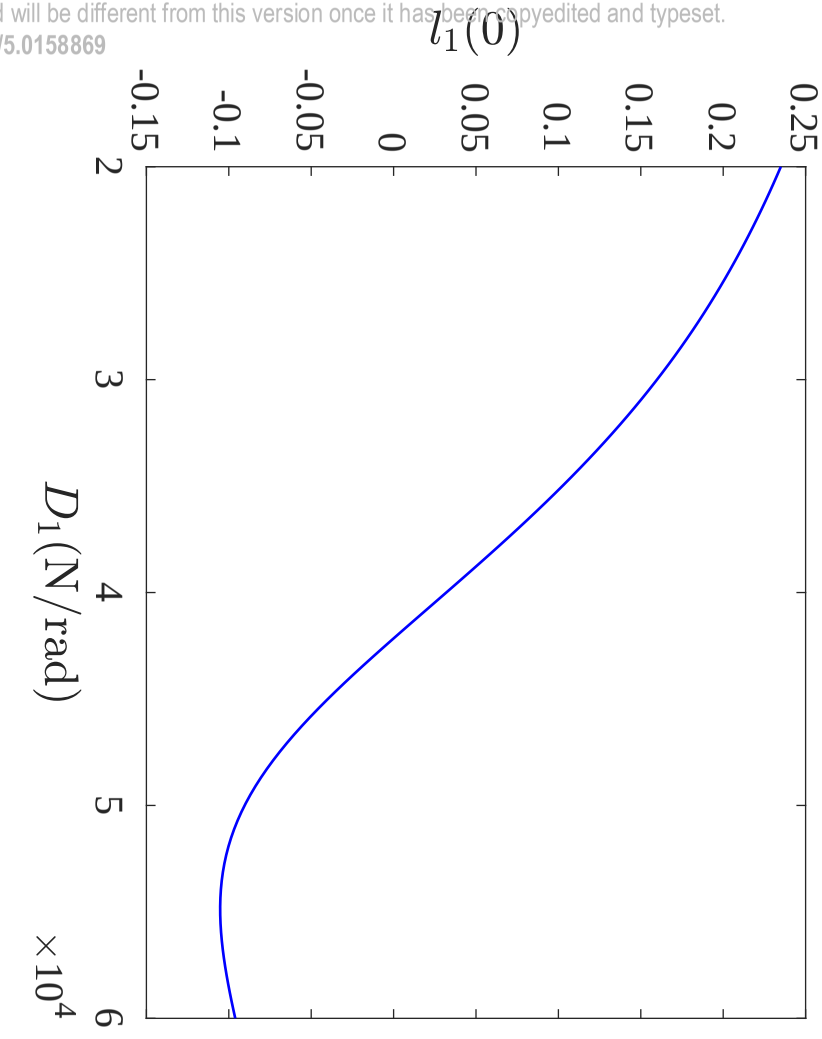

AIP Publishing

Chaos
An Interdisciplinary Journal
of Nonlinear Science

PLEASE CITE THIS ARTICLE AS DOI: 10.1063/5.0158869

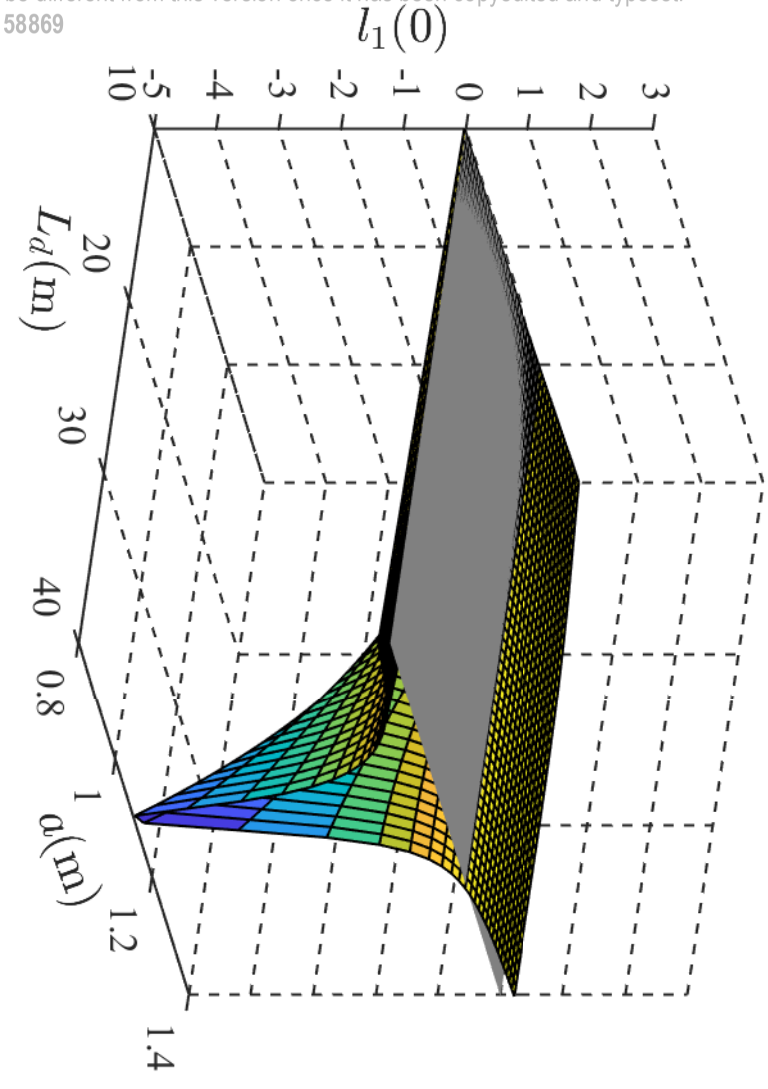

AIP Publishing

Chaos
An Interdisciplinary Journal
of Nonlinear Science

PLEASE CITE THIS ARTICLE AS DOI: 10.1063/5.0158869

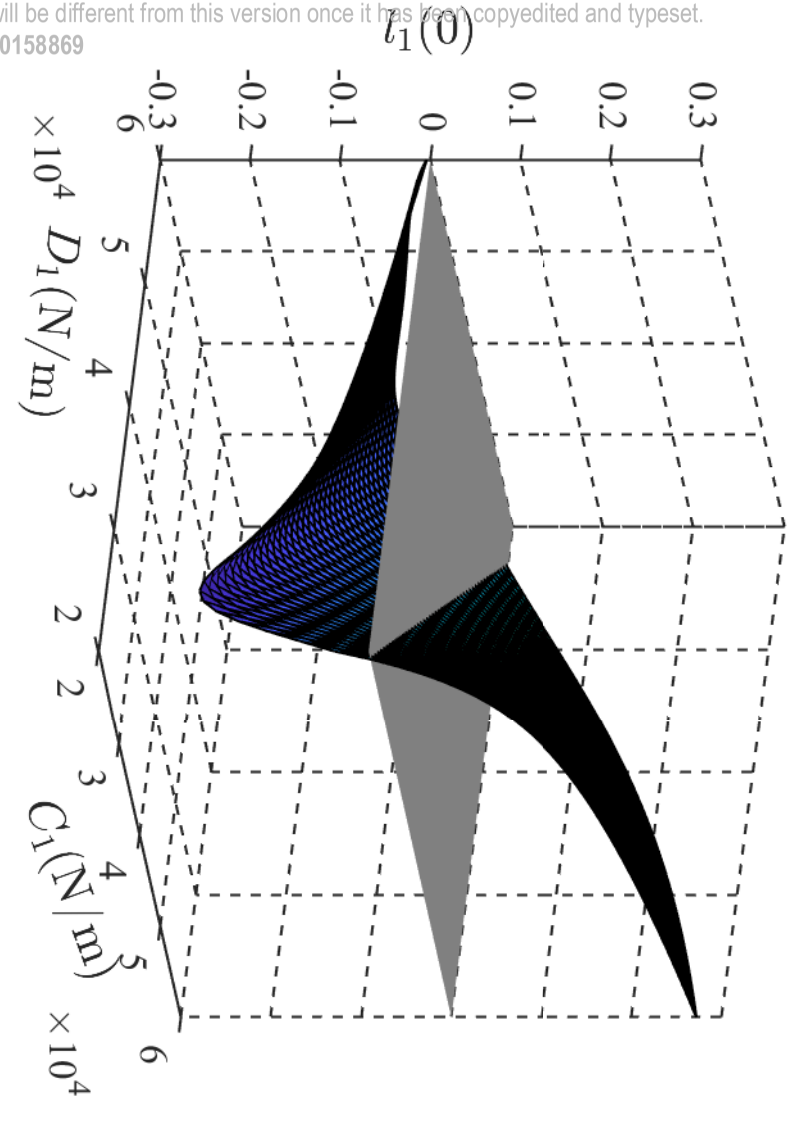

AIP Publishing

Chaos
An Interdisciplinary Journal
of Nonlinear Science

PLEASE CITE THIS ARTICLE AS DOI: 10.1063/5.0158869

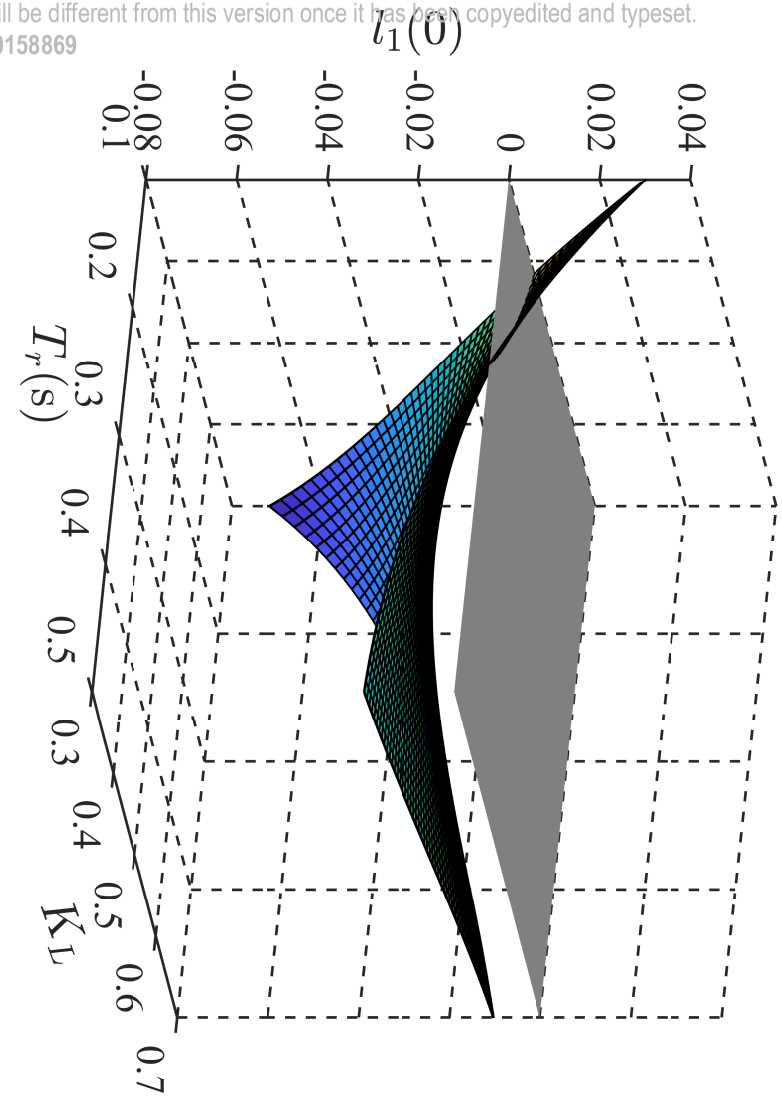

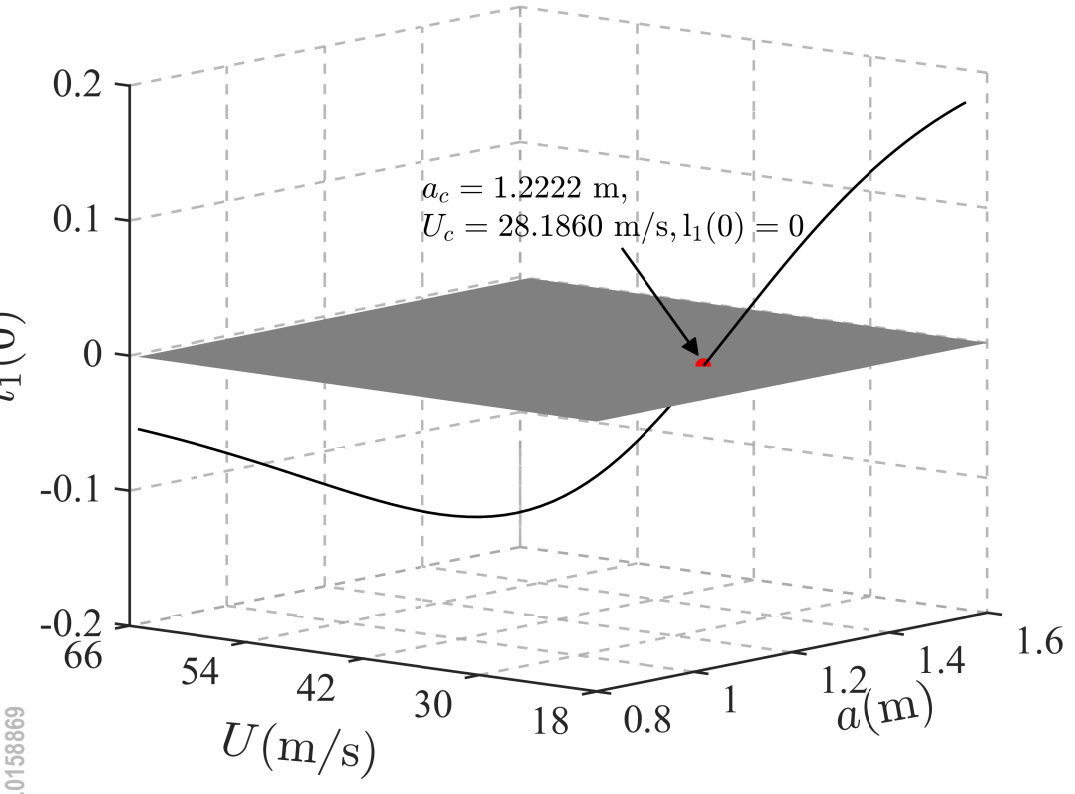

Chaos
An Interdisciplinary Journal
of Nonlinear Science

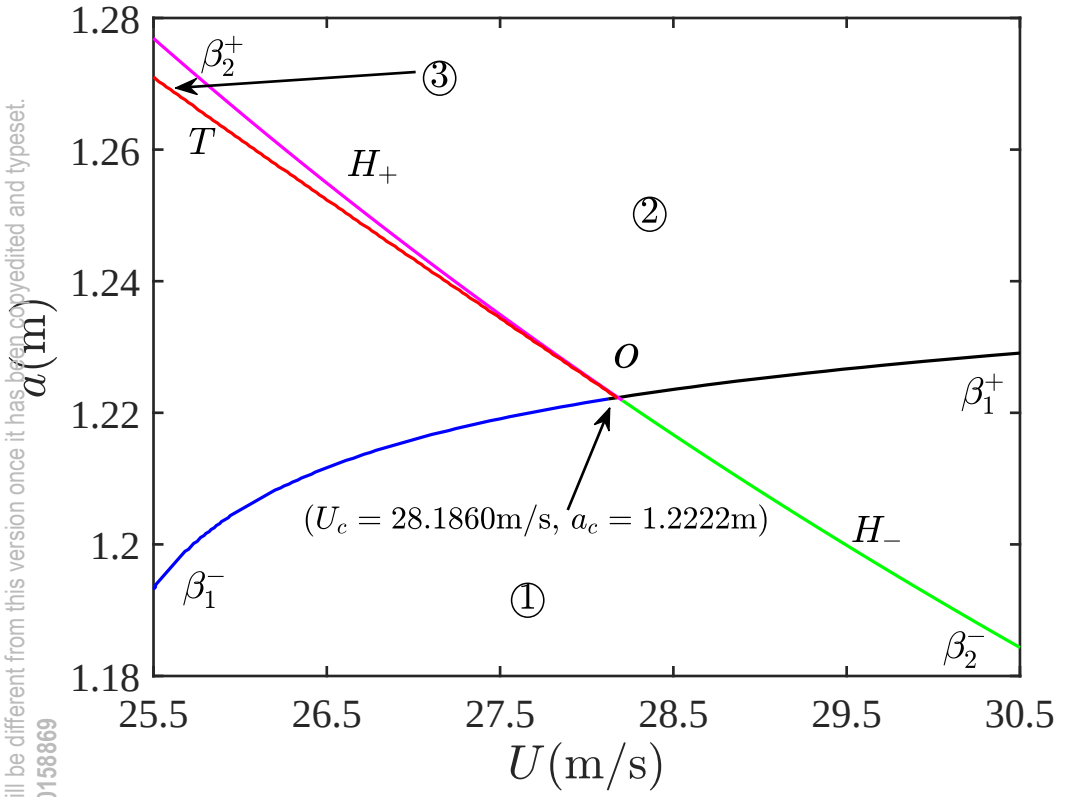

AIP Publishing
Chaos
An Interdisciplinary Journal
of Nonlinear Science

PLEASE CITE THIS ARTICLE AS DOI: 10.1063/5.0158869

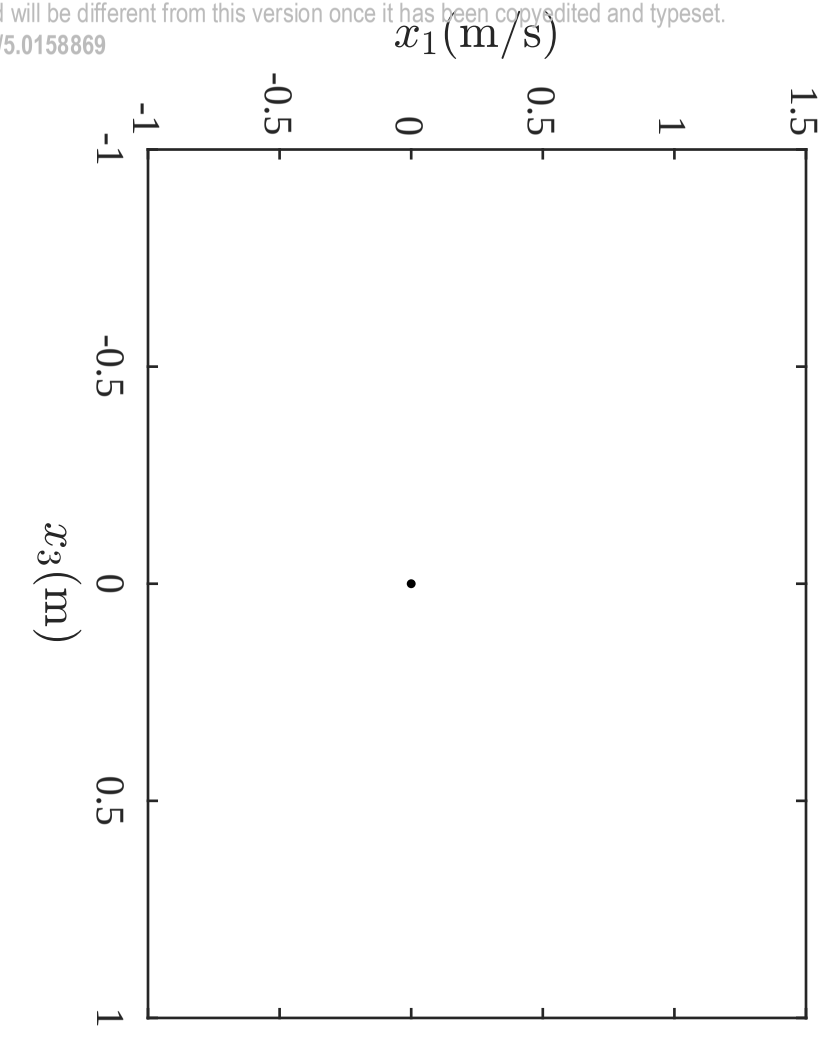

AIP Publishing

Chaos
An Interdisciplinary Journal
of Nonlinear Science

PLEASE CITE THIS ARTICLE AS DOI: 10.1063/5.0158869